atmosphere

MDPI

Article

Development and Evaluation of the Online Hybrid Model CAMx-LPiG

Andrea Piccoli [1,2,*], Valentina Agresti [1], Giovanni Lonati [2] and Guido Pirovano [1]

[1] Sustainable Development and Energy Sources, Ricerca sul Sistema Energetico—RSE Spa, Via R. Rubattino 54, 20134 Milan, Italy; valentina.agresti@rse-web.it (V.A.); guido.pirovano@rse-web.it (G.P.)
[2] Department of Civil and Environmental Engineering, Politecnico di Milano, Piazza L. Da Vinci 32, 20133 Milan, Italy; giovanni.lonati@polimi.it
* Correspondence: andrea.piccoli@rse-web.it

Abstract: CAMx-LPiG (Comprehensive Air Quality Model with Extensions—Linear Plume in Grid) is an online hybrid model based on the Chemistry and Transport Model (CTM) CAMx, which includes a sub-grid scale module to simulate the dispersion of linear road traffic emissions called LPiG. LPiG is a plume in grid module specifically developed by extending the capabilities of the Lagrangian puff sub-grid model available in CAMx. The online integration of the local scale model within the Eulerian CTM allows for a multiscale simulation of air quality from the regional scale to the urban scale, preserving a coherent description of the chemical state of the atmosphere at all spatial scales and avoiding any double counting of the emissions simulated by the sub-grid module. In this work, the model is presented and evaluated against measured NO_2 concentrations for the city of Milan for the month of January 2017. The model can introduce road traffic-induced gradient in NO_2 concentration at sub-grid resolution. Moreover, CAMx-LPiG has been shown to reduce bias compared to CAMx stand-alone simulations.

Keywords: air quality; hybrid modelling; road traffic; plume in grid; CAMx; urban air quality

Academic Editors: Jun Yang, Ling Han and Zhaobin Sun

Received: 3 March 2025
Revised: 30 April 2025
Accepted: 15 May 2025
Published: 16 May 2025

Citation: Piccoli, A.; Agresti, V.; Lonati, G.; Pirovano, G. Development and Evaluation of the Online Hybrid Model CAMx-LPiG. *Atmosphere* **2025**, *16*, 604. https://doi.org/10.3390/atmos16050604

1. Introduction

Most of the world's population lives in urban areas and this trend is projected to increase from 55% to 68% by 2050 [1]. High population density and a large number of activities lead to several environmental issues and exposure to high levels of atmospheric pollutants concentration for urban residents. Air pollution's impact on human health should be a major concern for policymakers. In 2018, long-term exposure to PM2.5 in the EU28 was associated with an estimated 251,000 to 495,000 premature deaths, while NO_2 exposure was linked to 31,000 to 76,000 [2]. These ranges reflect the 95% confidence intervals. As stated by the European Environment Agency (EEA), improving air quality in urban areas should be a priority [2]. With the latest WHO air quality guidelines on exposure to air pollution [3], 94% of the EU urban population exceeds the guideline value for NO_2 and 97% for $PM_{2.5}$ [4].

Among all pollution sources, road traffic has one of the highest impacts, especially in urban areas. According to emission data in EU countries, road transport is the main source of NOx emissions (39%) and the fourth for PM_{10} emissions (10%) [4]. In terms of ambient concentration, road traffic is estimated to be responsible for 72% of NO_2 and for more than 50% of PM_{10} in the municipality of Milan [5].

Road traffic emissions have been decreasing since the year 2000 [2], and it is expected that technological improvement of vehicles, together with urban mobility policies, will result in a further reduction in coming years. In Europe, the Green Deal aims to reduce 90% of transport-related greenhouse gas emissions by 2050, with only zero-emission new cars to be sold starting in 2035 [6]. The application of this policy would imply a swift transition from internal combustion vehicles to electric ones. A reliable quantification of the environmental impacts of this transition is crucial since it could help policymakers in their decision processes. To this end, chemical transport models (CTMs) of atmospheric pollutants could be a useful tool. Moreover, under the new revised "European Directive on ambient air quality and cleaner air for Europe 2024/2881", air quality modelling is set to have a central and expanded role in evaluating air quality within Europe, for example, from the development of air quality plans to the assessment of natural sources.

Eulerian CTMs are suitable for regional case studies, but they are not accurate enough to simulate urban dispersion phenomenon (i.e., road traffic emissions) because of their spatial resolution (e.g., highest resolution for CTMs ~1 km vs. maximum single lane width in Europe ~3.75 m [7]). To improve the accuracy of the simulation for local sources, different models are needed, such as Gaussian, puff, CFD (Computational fluid dynamics), Lagrangian, and street-specific box models. However, a limitation of stand-alone local models is their simplified approach to handling interactions between the contribution of local source to ambient concentrations and background concentrations. A multiscale hybrid approach, which combines Eulerian CTM with local sub-grid models, would be a good solution. Nowadays, the combination of CTMs and sub-grid models is one of the main challenges in air quality model research [8]. This coupling of models can be offline, when the two models are run independently and results are combined after a post-processing phase, or online, meaning that the models interact during the simulation and the final output includes the effects of both modelling tools.

In recent years, several studies about offline hybrid modelling techniques have been published [9–15]. Other examples of off-line hybrid approaches are SHERPA-CITY [16] and UTAQ [17] modelling systems, both implementing a Gaussian kernel approach to compute pollutant concentration at the urban level. The two systems are designed to provide fast screening analysis of long-term abatement strategies (SHERPA-CITY) and short-term forecasts (UTAQ). Background concentrations for both modelling approaches are derived from large scale Eulerian models, after removing the contribution of the sources explicitly simulated by the Gaussian module.

These offline approaches face two main challenges: (i) avoiding double-counting emissions and (ii) accurately simulating atmospheric reactions that produce secondary pollutants, both of which require complex post-processing. On-line hybrid models can overcome these issues. Among hybrid models, we mention Gaussian models (PinG) [18], box models (MUNICH) [19–21] or both (EPISODE City Chem) [22] combined with an Eulerian CTM that is developed specifically to improve the dispersion modelling of road traffic emissions. Another approach presented by Wang et al. [23] is the combination of LES (Large Eddy Simulation) models with the WRF-Chem model (The Weather Research and Forecasting [24,25]) to simulate concentration at high resolution in urban areas, without an explicit module for road traffic emission. In particular, the double counting issue in hybrid on-line models is solved by dumping the pollutant mass of the linear source that is being simulated at the end of each timestep to the CTM grid (PinG, EPISODE City-Chem) or by a two-way exchange of pollutants at rooftop height between the box model and the Eulerian component after a fixed time is passed (MUNICH). With regard to chemistry, MUNICH implements the full CB05 chemical kinetic mechanism whilst a

simplified approach for atmospheric chemistry is applied to the local dispersion module in PinG and Episode City-Chem.

This study introduces a novel extension of the CAMx Plume in Grid (PiG) module, called Linear Plume in Grid (LPiG), designed to handle linear emission sources such as road traffic with a sub-grid approach within the Eulerian CAMx model (Comprehensive Air Quality Model with Extensions). CAMx LPiG is specifically developed to be used along with the bottom-up emission modelling chain that we developed in previous works [26]. The objective is to develop a modeling tool capable of accurately assessing the impact of mobility policy scenarios on air quality. By integrating linear source geometry into PiG, the LPiG module provides a multiscale approach for simulating dispersion and transformation processes from local to regional scales. PiG techniques are usually applied to large point sources and have a long history of applications in CTMs [27]. Few approaches using PiG modules to treat road traffic are available in the literature and follow different approaches, from the discretization of roads with a high number of point sources [28] to the implementation of a Gaussian plume model for linear sources [18]. In this work, we modified the original PiG module to extend its capabilities to deal with road traffic emissions, thanks to the inclusion of linear source geometry in PiG. This work introduces some elements of novelty compared with the hybrid models available in the literature. First, the LPiG model implements a Super Gaussian formulation to the puff sampling in order to describe the characteristics of a road source in a dispersion model, the first application of this kind. Moreover, the local scale model for the simulation of road sources is fully on-line with a CTM, an approach which is implemented only by a handful of models [18–22]. Lastly, the model is implemented in CAMx, a state-of-the-art CTM widely used in air quality studies [29–33] and is easily implementable by CAMx users since it keeps the same convention for input files. This tool aims to enhance air quality modeling in urban areas by offering a flexible, reliable, and efficient solution.

Section 2 describes the modifications to the PiG module of CAMx, the modeling system, and the study case. Section 3 presents the hybrid model's application results and evaluation, while Section 4 discusses the model's performance.

2. Materials and Methods

The new hybrid module CAMx-LPiG is an extension of the bottom-up modelling chain presented in [26] and developed to assess the road traffic impacts on emission, air quality, and human health. The bottom-up modelling chain allows for a high-resolution estimation of traffic emissions, down to road-link level. The new optional module LPiG, here presented, explicitly simulates the dispersion and chemical transformation of the emissions of each road link, handled as a linear source, thus allowing for high-resolution analysis of the road traffic contribution to atmospheric pollution. The updated modelling chain is presented in Figure 1, with the new contribution presented in this work shown in orange. LPiG has been implemented in CAMx while trying to minimise the modifications to the original code, so it could be easily used by all CAMx users to explicitly simulate the local contribution to atmospheric pollution of road traffic.

Along with the hybrid module, this work also presents a new preprocessing module to reduce the computational burden of the hybrid air quality simulation. As presented in Section 2.2.3, the preprocessing module reduces the overall number of road links considered while maintaining the road network geometry.

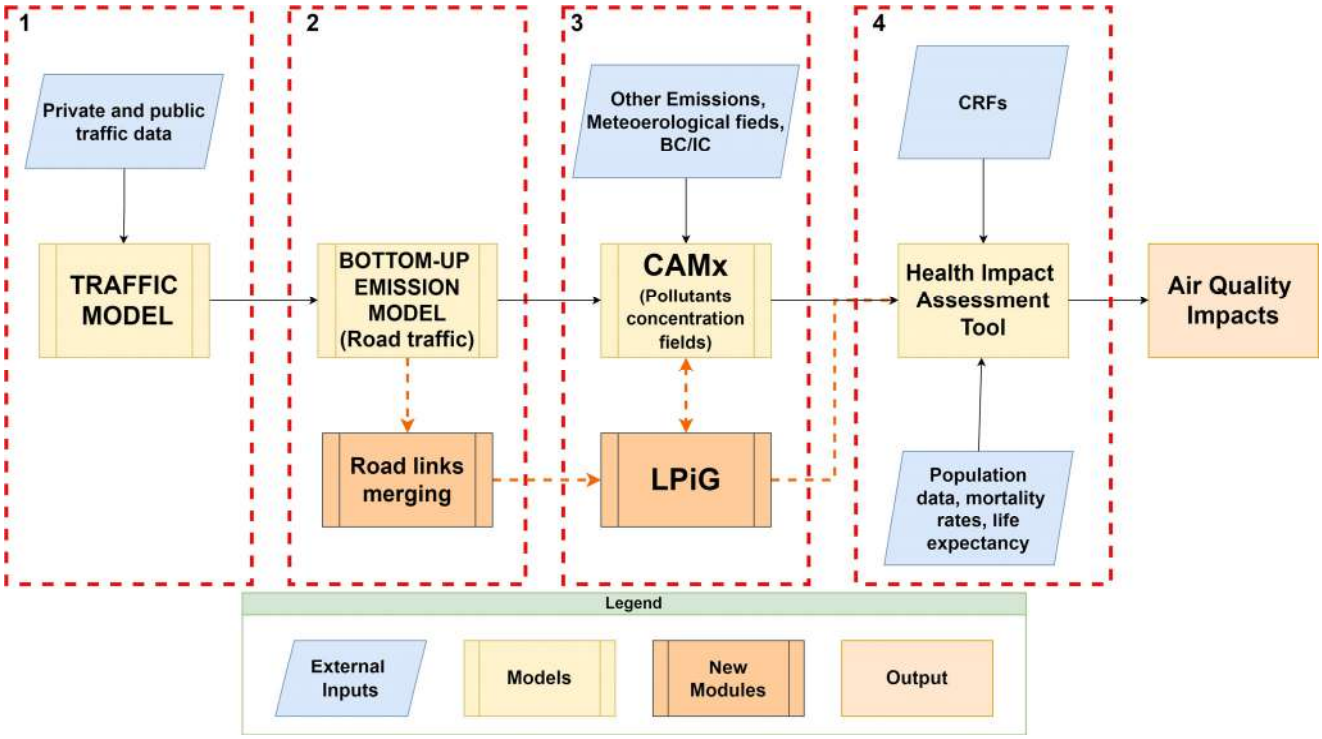

Figure 1. Flow chart of the bottom of the emission modelling chain with the new hybrid module LPiG (in orange).

2.1. LPiG Description

The Linear Plume in Grid Module (LPiG) is based on the original Plume in Grid (PiG) module [34] of the CAMx model. The original CAMx-PiG module is a Lagrangian Puff scheme, based on the SCICHEM model [35], which aims to simulate the emissions dispersion from single stacks at the sub-grid scale. The idea behind the CAMx-LPiG development is to create a PiG-like module capable of simulating the first phases of road traffic emissions dispersion at the sub-grid scale. In designing the LPiG code, we tried to keep as much as possible of the PiG code structure to make the CAMx-LPiG module simple, robust, and user friendly. Furthermore, LPiG input files are similar to PiG ones, except for some LPiG specific variables (Appendix D). For consideration of atmospheric chemistry, CAMx-LPiG implements both chemistry options already available for the original PiG scheme, namely:

- Greatly Reduced Execution and Simplified Dynamics (GREASD), which is a simplified NOx chemistry scheme developed for a computationally efficient treatment of early life plume chemistry, also including basic PM chemistry.
- Incremental Reactions for Organics and NOx (IRON), which is a more complete chemistry scheme for gas species but does not include PM chemistry.

The key features of the CAMx-LPiG sub-model are presented in the following subsection and appendixes addressing: the initial puff size and its evolution (Section 2.1.1), the changes in the puff release intervals to reduce the computational burdens (Appendix B), and the update of the GREASD chemistry option for LPiG puffs (Appendix C). Finally, the LPiG input files' structure is described in Appendix D.

2.1.1. LPiG Formulation

The original CAMx-PiG scheme simulates the dispersion of a point source emission as a stream of puffs released into the atmosphere. At the end of the emission period, each puff has longitudinal length and directional orientation defined by the position of the so-called

leading point L and trailing point T, which represent the endpoints of the puff in the wind direction. In the advection phase of the subsequent time steps, these points are transported according to the wind fields, thus changing the position of the puff centre point (i.e., the point midway the endpoints), stretching its shape, and varying its centerline orientation.

The CAMx-LPiG scheme follows the same approach but introduces some relevant modifications in the setting of the puff conditions in order to properly handle a linear source (i.e., a road segment). It is important to note that, in this first release of LPiG, the puff dispersion is simulated considering the streets as "open road", therefore not considering any effects due to surrounding buildings on street level airflow and road canyon effects (the presence of buildings on both sides of a road introduces local recirculation patterns that affects the dispersion of pollutants within the road canyon). Consequently, so far, it can be used to provide a first guess evaluation of the local contribution of each road segment with respect to other sources. This choice has been supported by the following reasons: (a) the sub-grid module allows, in any case, the key features of the release of road traffic emissions to be reproduced while avoiding the strong dilution that instantaneously spreads the emission over an area of, at least, 1 km^2; (b) this implementation does not require additional input data to be introduced, such as the description of the urban canopy geometry and specific high resolution meteorological data; (c) the same approach has been implemented in other air quality planning and managing tools such as SHERPA-CITY [16] and UTAQ [17]. It is worth noting that both online and offline modeling systems incorporating street canyon effects are available [9,22,36,37]. Meanwhile, the canopy effects on local meteorology can be addressed using more advanced parametrisation in meteorological modelling, such as the WRF-UCM (Weather Research and Forecasting Model—Urban Canopy Model) [38].

First of all, a simplification in the puff shape is necessary. Thinking of the linear source as a sequence of aligned point sources, at the end of the emission periods the puffs emitted by these sources will cover a surface ("smoke surface") on the horizontal plane determined by the puff mean motion. The basic idea for CAMx-LPiG development is to mimic this smoke surface using one single "synthetic" puff (synpuff) emitted by one single point source (named the "associated point source"). This point source is located in the centre of the road segment and has the same emission rate of the road. The position of the centre point of the synpuff, its size (i.e., the length of its major and minor axis), and its orientation at the end of the emission period are calculated and accounted for during the whole puff life to simulate the dispersion of the linear source emission. The smoke surface of the point sources sequence is depicted in blue in Figure 2 for a generic wind direction (α) relative to the street orientation. As shown in the figure, the resulting area will be a parallelogram unless α is equal to 0 or $\frac{\pi}{2}$. Since 2D Gaussian puff sampling takes place along two perpendicular axes, we simplified the smoke surface at the end of the emission timestep of the associated point source into a rectangle, conserving the smoke surface area and the position of its center point, which is used in CAMx-PiG to locate the puff in the sampling grid.

The resulting simplified smoke surface is represented in green in Figure 2.

The puff dimensions are defined by the length of the two axes. The first dimension, $L_{E1,s}$, is normal to the road orientation, while the second dimension, $L_{E2,s}$, is parallel to the road. For all values of α different from 0, $L_{E1,s}$ is computed to preserve the smoke surface area, while $L_{E2,s}$ is equal to the road length (L_S). $L_{E1,s}$ accounts for both the mean wind advection and the road width, and is computed as follows:

$$L_{E1,s,0} = \left|\underline{x}_{T,0} - \underline{x}_{L,0}\right| \sin\alpha + W_s \quad (1)$$

with $|\underline{x}_{T,0} - \underline{x}_{L,0}|$ being the distance between the leading and trailing point of the original smoke surface (the red dotted line in Figure 2) and Ws the road width. If α is equal to zero, $L_{E1,s}$ is equal to the road width W_S, while $L_{E2,s}$ accounts for L_S and the advection:

$$L_{E2,s,0} = |\underline{x}_{T,0} - \underline{x}_{L,0}| + L_s \quad (2)$$

Two additional figures that depict the limit cases of α equal to 0 and $\frac{\pi}{2}$ are available in the Supplementary Materials Section S1.

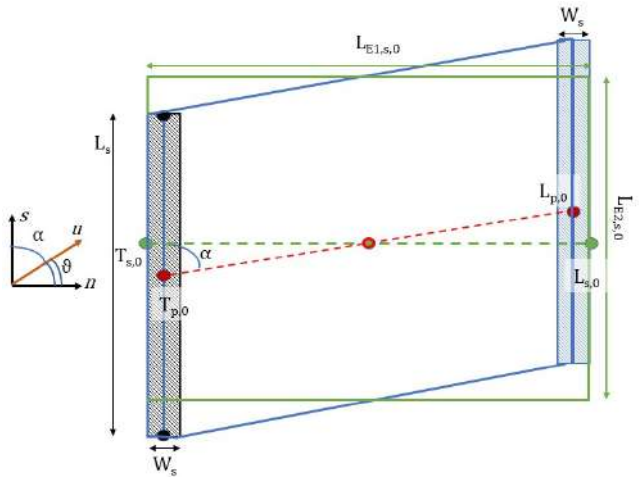

Figure 2. Definition of the puff geometry in case of generic wind direction. The road segment is reported as the black striped area, the leading and trailing points of the associated point source are in red, while the leading and trailing points of the street source are in green. The quadrilaterals in blue and green represent the initial smoke surface due to the mean motion of the puff for the associated point source and the street source, respectively.

During the time steps that follow the emission, the synpuff is subject to advection due to the mean wind condition. During the advection phase, the synpuff modifies its shape due to the variation in the distance between the leading point and the trailing point in the case of non-uniform mean velocity. The original CAMx-PiG algorithm is used to perform the advection along the synpuff x– and z–axes, whilst along the y–axis the synpuff length is recomputed during the puff life based on the following assumptions:

1. The synpuff volume V is constant during the advection phase.
2. The synpuff has the shape of a parallelepiped with sides L_x, L_y, L_z.
3. The relative change in the plume spread along the puff's minor axis matches the relative change in the length of the minor axis.

Assumptions 1 and 2 make it possible to write the balance equation for the synpuff volume for two subsequent time steps (t = 1, 2) of the advection period:

$$V_{t1} = V_{t2} \text{hence } L_{x,t1} \cdot L_{y,t1} \cdot L_{z,t1} = L_{x,t2} \cdot L_{y,t2} \cdot L_{z,t2} \quad (3)$$

where the variables L_x, L_y, and L_z depend on the synpuff size at the end of the emission period (i.e., $L_{E1,s}$ and $L_{E2,s}$) and on the turbulent dispersion coefficients (σ_x, σ_y, and σ_z) along the same direction:

$$L_x = L_{E1s} + 3\sigma_x,\ L_y = L_{E2s} + 3\sigma_y,\ L_z = 3\sigma_z \quad (4)$$

During the advection phase, $L_{E1,s}$ is modified due to the advection of the leading and trailing points of the puff according to the corresponding local wind conditions. To keep the puff volume constant, the minor effective length $L_{E2,s}$ needs to be modified accordingly.

Finally, at the end of each CAMx timestep, to evaluate the contribution of each linear source at the sub-grid level, the puff concentration is sampled with a user-defined high-resolution grid. CAMx-PiG computes the sub-grid concentrations assuming that the spatial concentration distribution within the puff can be approximated by a 2D Gaussian formula, where the concentration C of a generic pollutant "$_l$" in the high-resolution grid "$_{hr}$" (ground-level fields) is expressed as follows:

$$C_{l,hr}(x,y) = \frac{M_l}{2\pi \frac{L_x}{3}\frac{L_y}{3}\sigma_z} e^{-\frac{1}{2}\left(\frac{(x-x_c)^2}{(\frac{L_x}{3})^2}+\frac{(y-y_c)^2}{(\frac{L_y}{3})^2}\right)} \quad (5)$$

where L_x and L_y are defined by Equation (4) and M_l is the mass of pollutant "l" enclosed in the puff volume. PiG supposes that the concentration is uniformly distributed along the vertical direction, therefore, there is no dependency from the z coordinate. The Gaussian formula assumes that the emission originates in a single point, while in our application we are interested in sampling a linear source with constant emission along its length. To achieve this, in CAMx-LPiG the sub-grid concentrations are computed using a Super Gaussian formula in the y direction:

$$C_{l,hr}(x,y) = \frac{M_l}{2\pi \frac{L_x}{3}\frac{L_y}{3}\sigma_z} e^{-\left(\frac{(x-x_c)^2}{2(\frac{L_x}{3})^2}+\left(\frac{(y-y_c)^2}{2(\frac{L_y}{3})^2}\right)^{P_y}\right)} \quad (6)$$

The Super Gaussian formulation was successfully used by Jia and Kikumoto to develop a source term estimation (STE) method for linear sources [39]. Figure 3 shows a comparison of the concentration sampling for a synthetic puff originating from a 200m linear source with $\sigma_y = \sigma_x = 10$ m along the y coordinate at the puff centre. The comparison is made using 200 Gaussian point sources, the Gaussian equation for a linear source, and the Super Gaussian function for two values of P_y. The Super Gaussian formula more accurately approximates the actual concentration pattern of the linear source. The best value of P_y depends on the road length and the values of α. Further details on P_y computation and the Super Gaussian implementation are given in the Supplementary Materials Section S2.

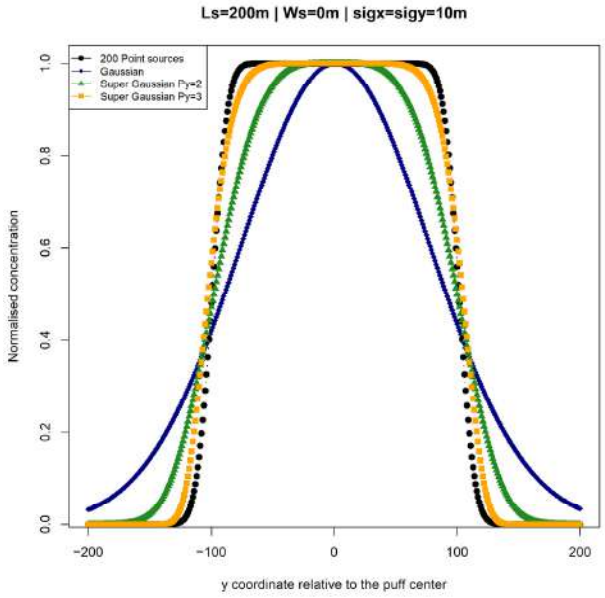

Figure 3. Comparison between the normalized concentration for 200 Gaussian point sources, the Gaussian equation for a linear source, and the Super Gaussian function for two values of P_y.

As highlighted in the initial condition settings, L_y is always aligned with the road direction. As explained in Appendix B, the lifespan of the puff is limited to a maximum of 10 min circa, thus limiting the changes in wind direction that might change the orientation of the puff. By using this formula, we can account for the uniform emission pattern of a road source while conserving most of the original CAMx-PiG structure.

2.2. Case Study Definition

2.2.1. Modeling Set-Up

The hybrid model based on the Eulerian CAMx model (version 7.1) with the Lagrangian CAMx-LPiG module was implemented for a case study in the city of Milan for the winter month of January 2017. The CAMx model was applied over two computational domains (Figure 4). The coarser domain (ITA) covers the Italian peninsula with 4 km of horizontal resolution and is composed of 284 × 364 cells and 14 terrain-following vertical levels. The finer nested domain (MIL) covers the metropolitan area of Milan with a 1 km resolution and is made up of 70 × 70 grid cells. CAMx-LPiG was applied to a 50-m resolution urban sampling grid (URB), covering the city centre of Milan and corresponding to four cells of the ITA domain.

Additional details on the CAMx setup are reported in Table 1.

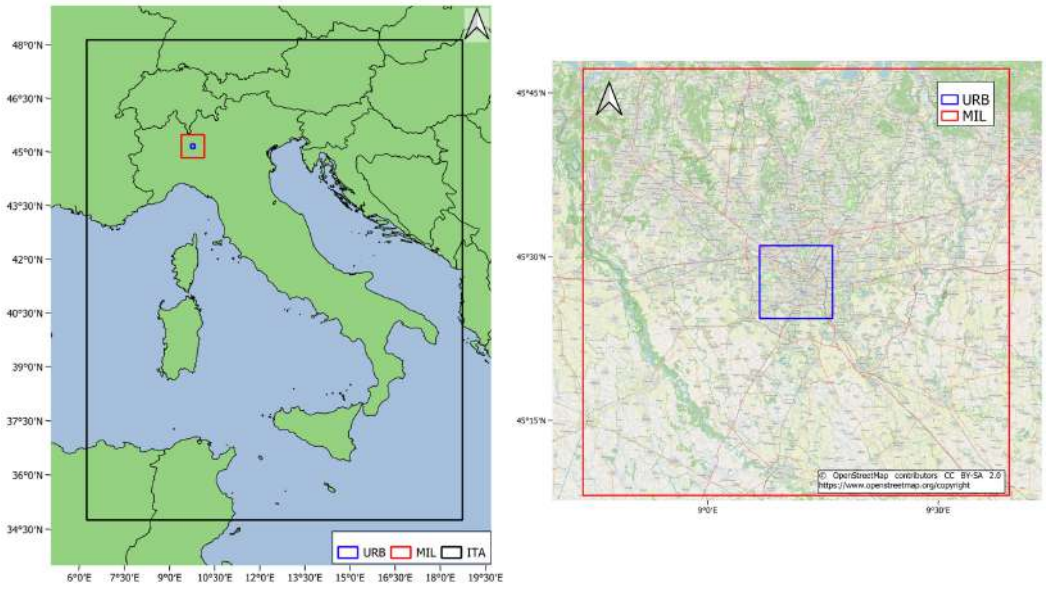

(**a**) (**b**)

Figure 4. Set of nested domains used in CAMx and high-resolution sampling grid for CAMx, at the national scale (**a**) and local scale (**b**). The coarse 4-km Italian domain (ITA) is depicted in black, the fine metropolitan 1-km domain (MIL) in red, and the 50-m high resolution grid (URB) for the sampling of the hybrid model in blue.

Table 1. CAMx main settings.

Parameter	Scheme
Chemistry scheme	CB05
Aerosol treatment	CF
Inorganic aerosol chemistry	ISORROPIA
Organic aerosol chemistry	SOAP2.2
LPiG chemistry option	GREASD
Dry deposition scheme	Zhang [40,41]

2.2.2. Meteorological and Emission Data

The air quality simulation was driven by meteorological input data obtained from a customized configuration of the numerical weather prediction (NWP) model Weather Regional Forecast (WRF) [24]. WRF data have the same spatial resolution for the ITA domain with a bigger extent (289 × 367 cells) to avoid boundary effects, but a slightly different resolution (1.33 × 1.33 km) for the MIL domain. Thus, the meteorological data for the MIL domain were obtained by downscaling the WRF output at 1.33 km to 1 km thanks to the WRFCAMX processor [34]. We set the vertical levels of the domains to 56.

Emission data from the Italian national emission inventory, providing data at the province administrative level for the year 2015, were used for the ITA domain [42]. For the MIL domain, we used data from the regional emission inventory of the Lombardy region INEMAR 2014 [43], which provides emission data at the municipality level recalibrated for the year 2017, however, road traffic emissions in the city of Milan have been computed with a dedicated bottom-up approach. Both the inventories were processed with the Sparse Matrix Operator for Kernel Emission model (SMOKE v3.5) [44] to obtain hourly gridded emission fields over the two domains. Biogenic and sea salt emissions for the ITA domain were estimated using the Model of Emissions of Gases and Aerosols from Nature (MEGAN v2.03) [45] and the SEASALT model [46], respectively. Biogenic emissions for the MIL domain were obtained by downscaling the 4-km MEGAN output. Boundary and initial conditions necessary for CAMx were obtained from the CHIMERE model using INERIS' Prev'Air service [47].

Road traffic emissions for the city of Milan (i.e., for the cells of the MIL domain covering the city) were purposely estimated according to an accurate bottom-up approach with HERMESv3_BU model (High-Elective Resolution Modelling Emission System version 3—Bottom up) [48]. The HERMESv3_BU model computes traffic emissions (both exhaust and non-exhaust, as well as dust resuspension) at high spatial (i.e., single road link) and temporal (i.e., hourly) resolution combining traffic activity data (traffic flow and mean vehicle speed data) with emission factors from Tier 3 methodology of EMEP/EEA [49], which correspond to the values reported by the European COPERT 5 model (https://copert.emisia.com/). In our work, emissions for both private and public transport were separately calculated: the former based on data from a simulation for private traffic carried out by the Environment and Mobility agency of the city of Milan (AMAT—Agenzia Mobilità Ambiente Territorio), the latter from public transport data available on the open data portal of the city of Milan [50]. Results were then summed to assess total emissions at the single road link level. A comprehensive description of the bottom-up approach for the estimation of road traffic emissions used in this work is available in [26].

At this stage, we simulated with CAMx-LPiG only the main streets within the URB domain in order to reduce the computational cost, thus, 1448 road links out of 19220 from the original road graph of the city of Milan were selected. The selected roads are the primary streets of the city centre, accounting for 14.32% of NOx emissions from road traffic in the city of Milan. The road graph was further simplified, as explained in Section 2.2.3. Figure 5 shows the road links explicitly simulated with CAMx-LPiG. The simulated road network considers the three ring roads of Milan city centre and the main connections between them. The innermost ring road is situated in a Low Emission Zone (LEZ—AREA C) where both congestion charging and restrictions based on Euro emission class and vehicle type are applied. Restrictions to the circulating fleet were considered while computing emissions using the HERMESv3_BU model in the LEZ zone, as described in [26].

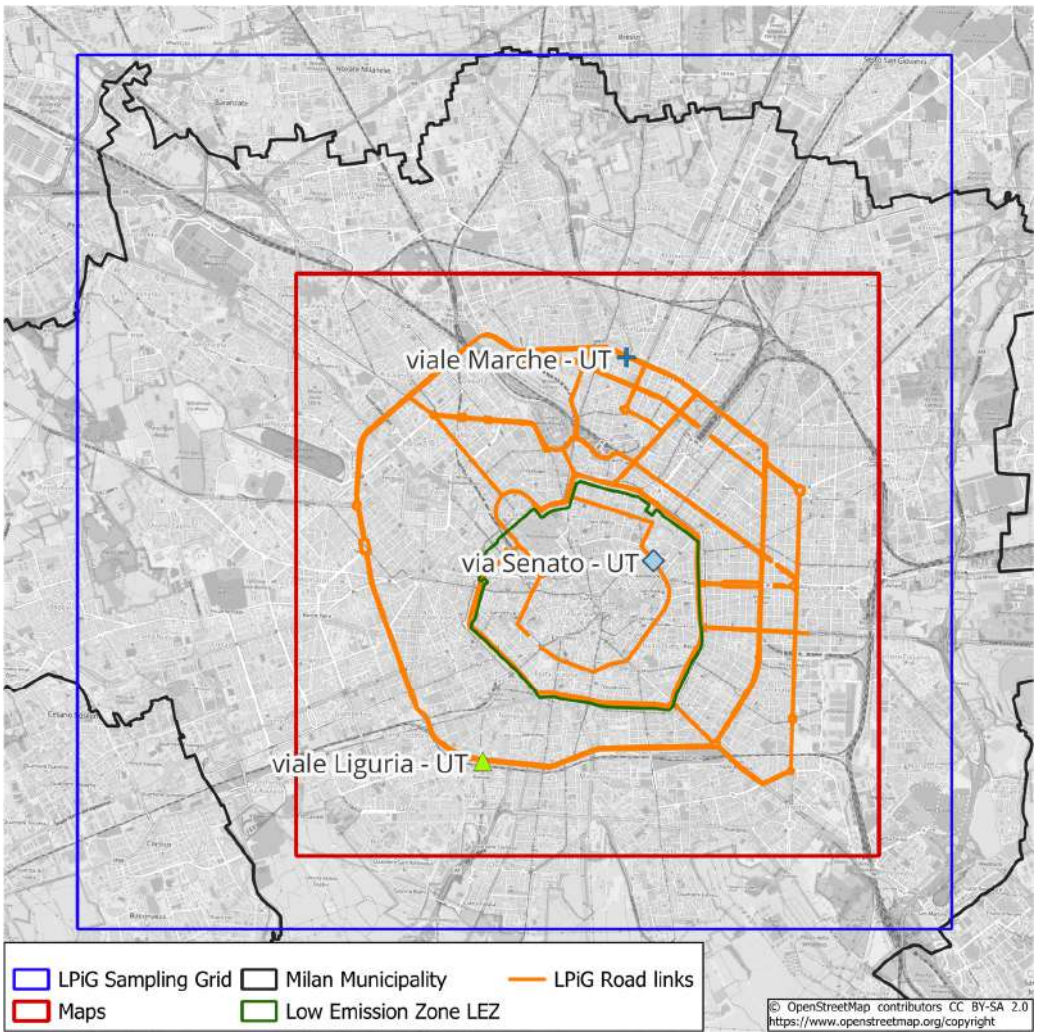

Figure 5. Road links simulated with the LPiG Module (orange), air quality stations used for model evaluation, border of Milan municipality (black), LPiG sampling grid (blue), Milan's LEZ AREA C (green), and the portion of the domain represented in the air quality maps (red), corresponding to Milan city centre.

2.2.3. Connection of CAMx-LPiG with the Bottom-Up Modelling Chain

The results of the bottom-up estimate of road traffic emissions were used to feed the hybrid model CAMx-LPiG, introducing additional processing steps aiming at: (a) simplifying the road network explicitly simulated with CAMx-LPiG (Figure 5) to reduce the computational burden of the LPiG module; (b) converting HERMESv3_BU output data into CAMx-LPiG format.

To achieve such goals, the following steps were put in place:

- Sum emission for public and private transport to one single file.
- Reduce the number of road links by merging consecutive road links that lie in straight lines and opposite direction lanes of the same carriageway (Figure 6). Road links were defined to be in a straight line if the angle between two consecutive links is less than 4.5°. We set a maximum length limit of 600 m for the newly merged roads.
- Sum emission for the merged links.
- Write the netCDF emission file for CAMx point sources for the merged links.

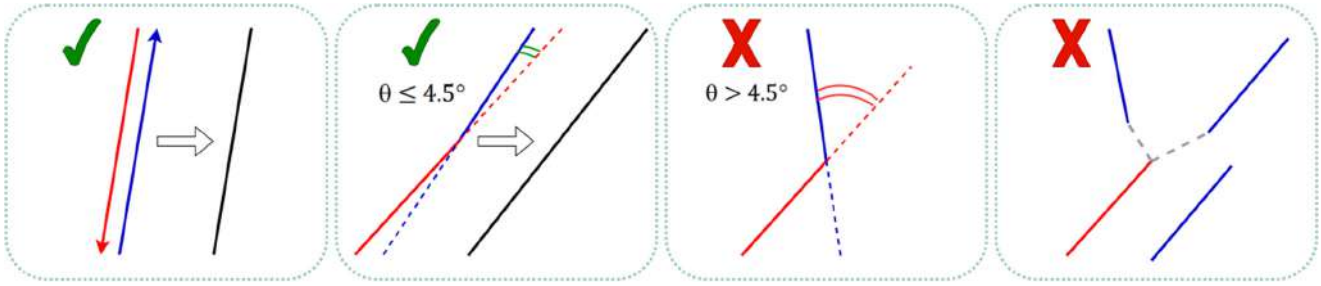

Figure 6. Merge example from point 2 and results. First panel: opposite direction links of the same carriageway. Second Panel: consecutive links with the angle between them less than 4.5°. Example of links that are not merged. Third panel: consecutive links with the angle between them greater than 4.5°. Fourth panel: non-consecutive links.

The merging operation reduced the number of links from 1448 to 547 while maintaining the overall road network geometry shown in Figure 5. For CAMx-LPiG road links, information on road width was necessary. The traffic model shapefile did not provide this information, so we used the number of lanes provided by another shapefile of the road network available on the Milan municipality's open data portal. Using the map matching algorithm Fast Map Matching (FMM) [51], we matched the road links of the two different shapefiles to retrieve information on the number of lanes for each LPiG road. Then, we assumed a standard width of 3.25 m for a single lane.

2.2.4. Model Evaluation Data

Simulations were separately performed with CAMx and CAMx-LPiG hybrid model for the month of January 2017. The results of the CAMx-LPiG application are evaluated against NO_2 concentration values to assess the hybrid model simulation performances. The CAMx-LPiG concentrations are also compared with the standard application of CAMx with the same inputs, meaning that road emissions are not separately processed but simulated directly by the Eulerian 1-km grid model.

The evaluation is focused on NO_2 because it is the main pollutant associated with road traffic and it is one of the most critical pollutants in urban areas, also showing relevant spatial gradients, mainly due to road emissions. Moreover, NO_2 is a reactive pollutant whose chemistry is explicitly evaluated by the GREASD scheme. For all these reasons NO_2 represents a key pollutant to investigate the model performance. Model evaluation for NO_2 is performed against data collected at three urban traffic monitoring sites of the regional environmental protection agency (ARPA) of Lombardy, represented in Figure 5. These monitoring sites are in close proximity to streets of the road network considered by the CAMx-LPiG module. In particular, sites S1 and S2 are located on the outer ring road of the city centre whereas site S3 is on the inner ring road in the Low Emission Zone. The characteristics of each monitoring site are reported in Table 2. Monitoring stations are not explicitly defined as sampling points in LPiG, however, the concentration at each air quality monitoring station is derived from the sampling grid cell of the URB domain in which the monitoring station is located.

Table 2. Air quality monitoring stations characteristics.

Site	Site Code	Name	Type	X (°)	Y (°)	Z (m asl)	Distance from LPiG Source	Low Emission Zone
S1	IT0477A	Viale Marche	Urban Traffic	45.4963	9.1909	129	11 m	No
S2	IT0761A	Viale Liguria	Urban Traffic	45.4438	9.1679	115	7 m	No
S3	IT1016A	Via Senato	Urban Traffic	45.4705	9.1974	118	5 m	Yes

In addition, results of the performance evaluation for NOx are presented in the Supplementary Materials Section S3. As at the local scale NOx can be considered as a primary pollutant, the evaluation of the model's performance in its reproduction is useful to assess the model's ability to simulate the dispersion mechanisms, neglecting the chemical transformation processes.

3. Results

3.1. Application of CAMx-LPiG

The plots of the monthly mean concentration fields for NO_2 over Milan city centre (referred to as "Maps" in Figure 5) computed by CAMx-LPiG and by the standard CAMx simulation are presented in Figure 7. The comparison between the model results clearly shows that the hybrid model can reproduce local concentration increments and gradients in the proximity of the road links simulated with the LPiG module, proving its ability to investigate the sub-grid concentration gradients inside the Eulerian model. In both model applications, the south-western part of the city centre presents higher concentration (in the order of 35 ppbV as the monthly average for January), but the CAMx-LPiG application estimates up to 4 ppbV higher concentrations (i.e., about 10%) than the standard CAMx in the proximity of the simulated road links. From the visual analysis of the maps of Figure 7, we can say that CAMx-LPiG is able to introduce concentration increments and gradients also in the western and northern parts of the area, reflecting the structure of the simulated road network. These gradients are proportional to the local traffic intensity, as shown by the difference in NO_2 concentration increments estimated for the major road links outside the LEZ area compared with the innermost road ring that is entirely within the LEZ area.

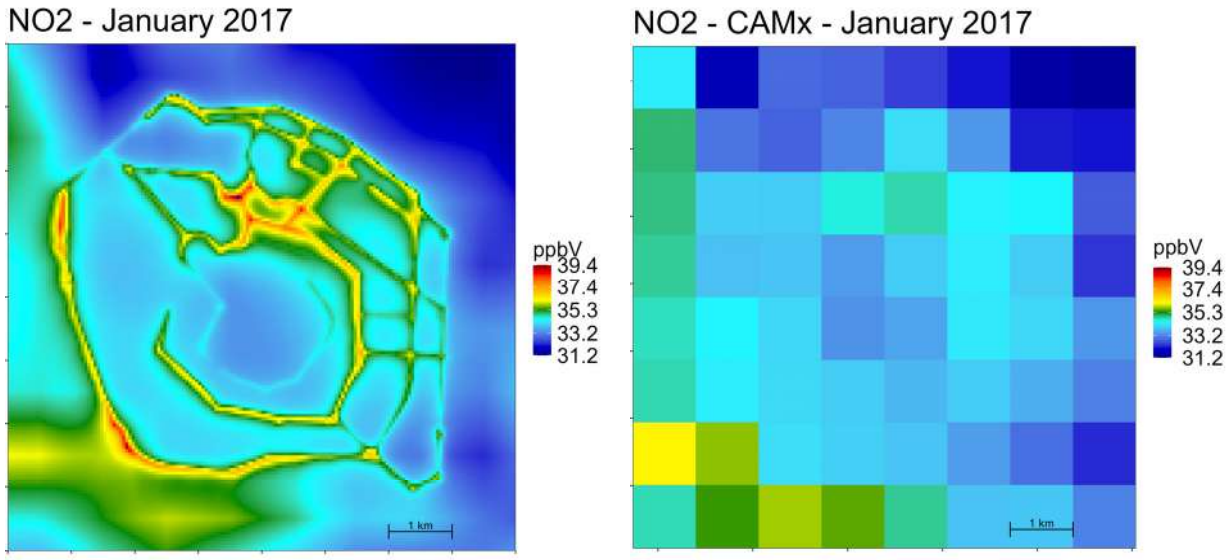

(**a**) (**b**)

Figure 7. CAMx-LPiG at 50m resolution (**a**) and standard CAMx (**b**) NO_2 monthly mean concentration for January 2017 over Milan city centre (referred to as "Maps" in Figure 3).

In order to evaluate the magnitude of such increments and the extension of the gradients, monthly mean NO_2 concentrations obtained through CAMx-LPiG simulation were sampled on 500 m-long transects perpendicular to the road links and analyzed. Overall, 308 transects were analyzed (Figure 8); for each transect, concentration data were

taken at 10 points approximately every 50 m. The local concentration increments $\Delta C_{i,j}\ (ppb)$ for each transect i and sampling point j were calculated as:

$$\Delta C_{i,j} = C_{i,j} - \min\left(C_{i,j}\right) \tag{7}$$

where C_i is the mean sampled concentration for January.

The local relative increment $\Delta Crel_{i,j}$ was computed as:

$$\Delta Crel_{i,j} = \left(\frac{C_{i,j}}{\min\left(C_{i,j}\right)} - 1\right)\% \tag{8}$$

$\Delta C_{i,j}$ and $\Delta Crel_{i,j}$ data were then pooled together into five 50-m long bins based on the distance from the road (L1-L5 and R1-R5, the farthest and the closest on the left and right side, respectively), and the resulted distributions are represented in the boxplots of Figure 9.

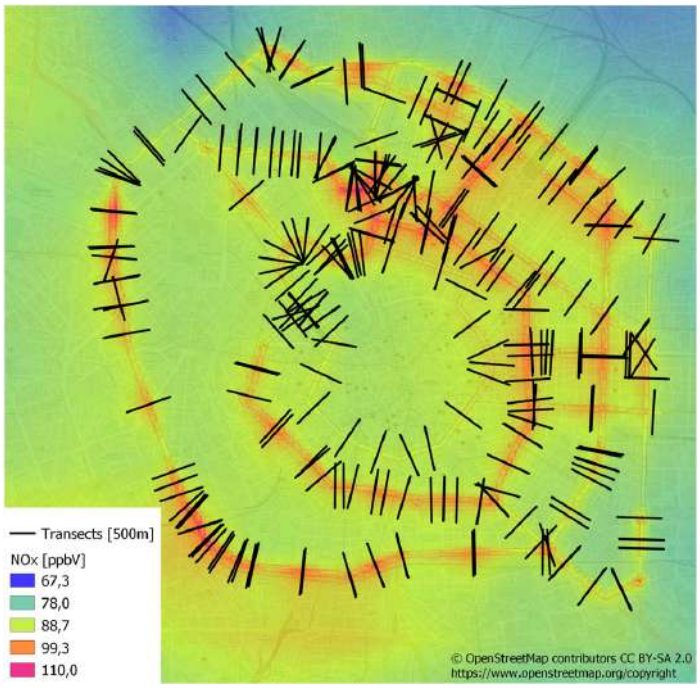

Figure 8. Sampled transects (black) and NOX concentrations.

As expected, the concentration increment sharply decreases moving away from the road on either side, reaching zero in its average value at a distance of 250 m (Figure 9). Along the first 50 m from the road, mean values for the concentration increment are in the order of 1.5–2 ppb (i.e., +5%), and mostly within the 1–2.1 ppb range, however, increments as high as 4–5 ppb (i.e., about +13%) have been estimated for some transects.

Despite the progressive reduction in road distance, significant increments (1.5–3 ppb, i.e., +5%–+10%) were sometimes obtained far away from the road too. This is because a transect can intersect one or more other road links so that the actual concentration increment profile is the result of the superimposition of increments from other roads that alter the typical exponential-decay profile of a single road link. Additionally, for high-trafficked roads, the length of the transects may be too short to bring the increments to zero, however, extending the transects further would only increase the chances of superimposition of road increments. Therefore, the 500-m transect length is a good compromise to appreciate the local contribution of road emissions in addition to background concentrations by means of the LPiG module.

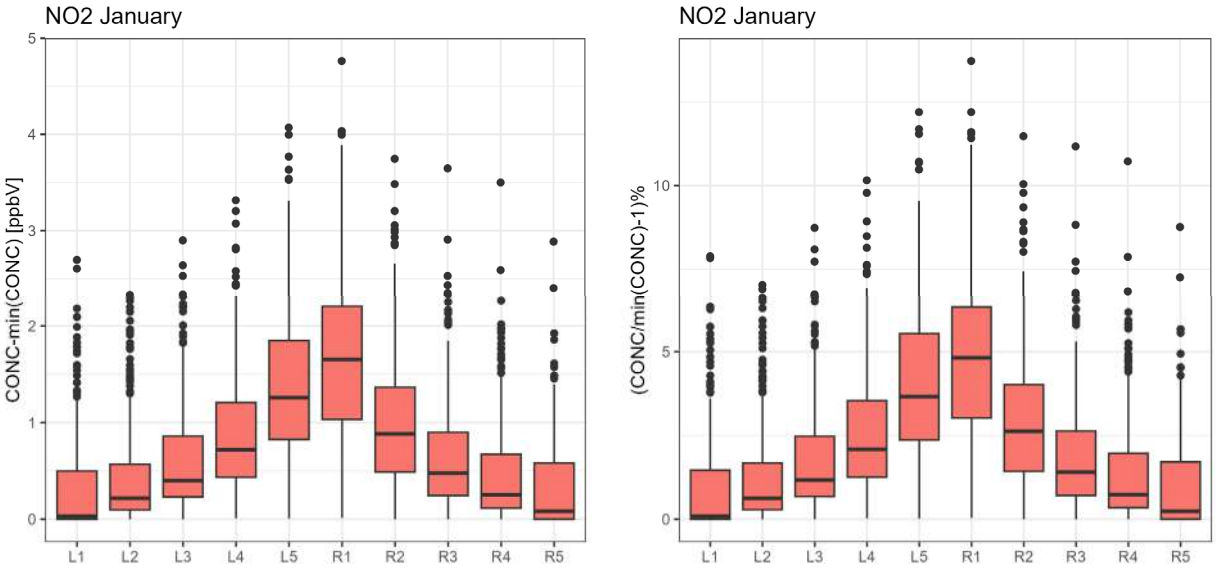

(**a**) (**b**)

Figure 9. Boxplots of local cross-road increment for NO_2 monthly mean concentration in absolute terms (ppbV, (**a**)) and relative terms (%, (**b**)).

3.2. Model Evaluation

3.2.1. Daily Concentrations

The time series of the observed and modelled NO_2 daily concentrations, both as CAMx and as CAMx-LPiG results, are shown in Figure 10 for the three monitoring sites for January 2017. At all sites, CAMx-LPiG provides slightly higher concentrations than CAMx. The increase in the monthly median simulated value ranges from a minimum increase of 0.5 ppb (34.7 ppb vs. 35.2 ppb) at site S3 to a maximum increase of 2.2 ppb (36.4 ppb for CAMx-LPiG vs. 34.2 ppb for CAMx) at site S2. However, the effect of the LPiG module becomes larger on high concentration days: with respect to CAMx simulation, the values of the 95th percentile of the daily concentrations show a maximum increase of 5.3 ppb at site S2 (52.3 ppb vs 47.0 ppb, i.e., +10%) and at site S1. The minimum increase is registered at site S3 with an increment of 2.2 ppb. The difference between CAMx-LPiG and CAMx output reflects the exposure to traffic emissions and the location of the monitoring sites. The concentration increment given by CAMx-LPiG is more evident at sites S1 and S2, located on the high-trafficked outer ring roads, and is lower at site S3, because of the lower volume of traffic that circulates in the LEZ with respect to the main ring roads.

During the first half of the month, model results are in fairly good agreement with the observations, both in terms of concentration values and of their time pattern. However, underestimations are observed on 5 January at all sites (about 10 ppb less than observed) and on 8–9 January (5 to 7 ppb less); conversely, overestimations ranging from 10 ppb at site S2 and S3 up to about 20 ppb at S1 occur on 12 January. From 13 January, the differences between observations and model results become more evident and systematic, even though the growing concentration trend until 25 January is reproduced by the models. These differences are due to a strong and sudden decrease of modelled concentrations ($-20/-30$ ppb) at all sites on 13–14 January, opposite to the trend of the observations. Finally, the observed and modelled time series tend to converge again during the last days of the month. However, some rather large discrepancies still occur on 26 January (negative bias) and on 27 January (positive bias), when model results show a peak around 50 ppb and the observed values are around 40 ppb.

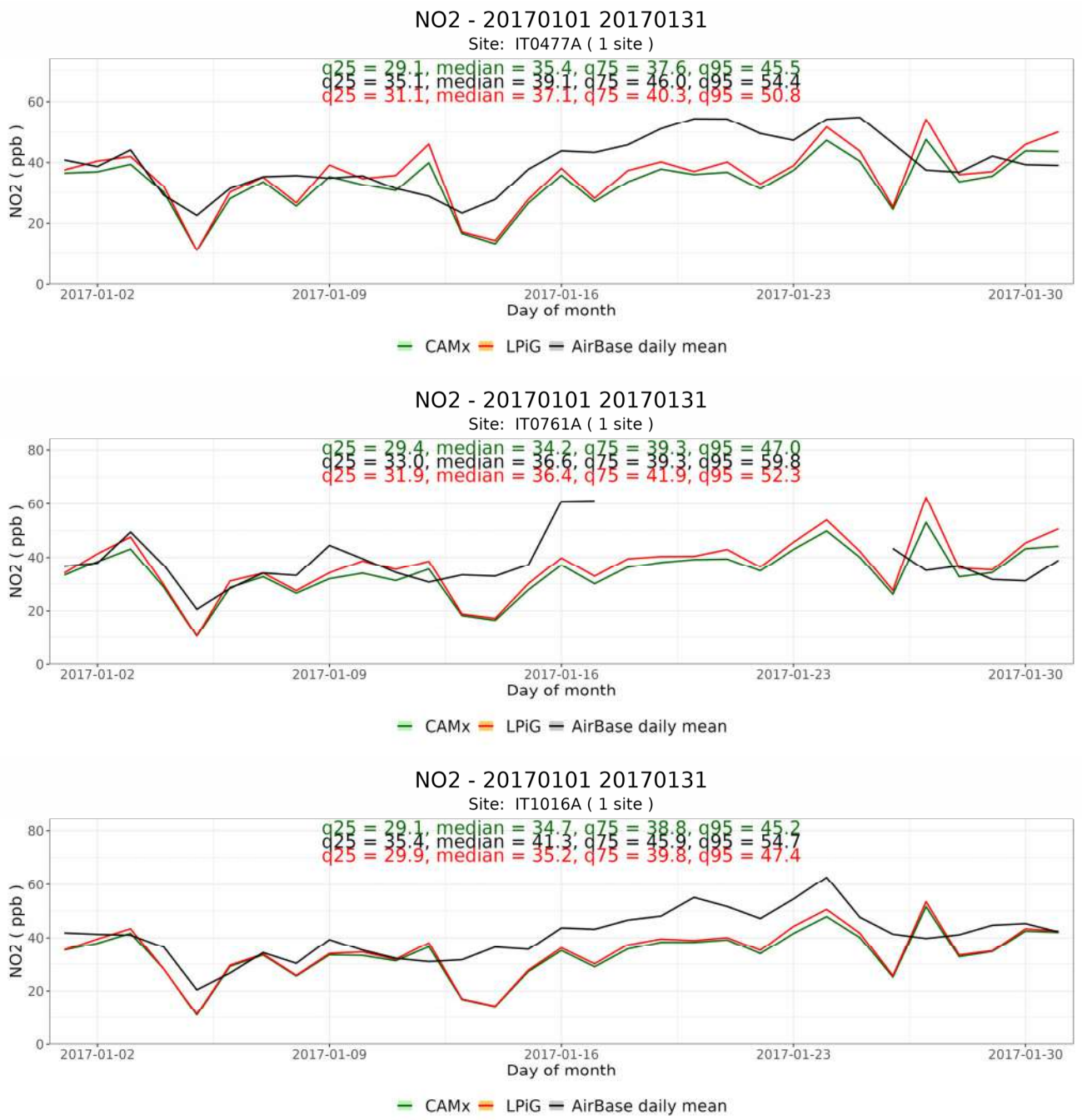

Figure 10. Time series of daily mean NO_2 concentrations at the AQ stations of Viale Marche (Site S1: IT0477A), Viale Liguria (Site S2: IT0761A) and Via Senato (Site S3: IT1016A) in January 2017 (black line: observed values; red line: CAMx-LPiG simulation; green line: CAMx simulation).

A comprehensive view of CAMx-LPiG performance is given in Figure 11, where NO_2 modelled concentrations are plotted against the corresponding daily mean observations at the three monitoring sites. Almost all (97.6%) of the model–observation pairs are within the FAC2 area (i.e., ±50%), and 81% within the lines with a slope of 0.7 and 1.42 (i.e., ±30%).

The values of performance indicators for the NO_2 daily means simulated by CAMx-LPiG for January 2017 are reported in Table 3. Overall, model results underestimate the observed concentrations at all sites: the observed monthly averages are in the 37.7–40.9 ppb range, whereas, modelled values are in the 34.6–35.7 ppb range. Values for the Mean Bias (MB) are −4.2 ppb at site S2, −2.7 at site S1, and −6.3 ppb at site S3; Normalized Mean Bias (NMB) values range between −15.5% (S3) and −8% (S2). The largest underestimation

(−6.3 ppb for the monthly average) is observed at site S3, where the observed values are at their highest level. Nevertheless, the highest values for correlation (COR = 0.68) and Index Of Agreement (IOA = 0.72) are obtained at site S3, followed by site S1 (0.51 and 0.69) and site S2 (0.3 and 0.53), where performance metrics suffer from the reduced data availability.

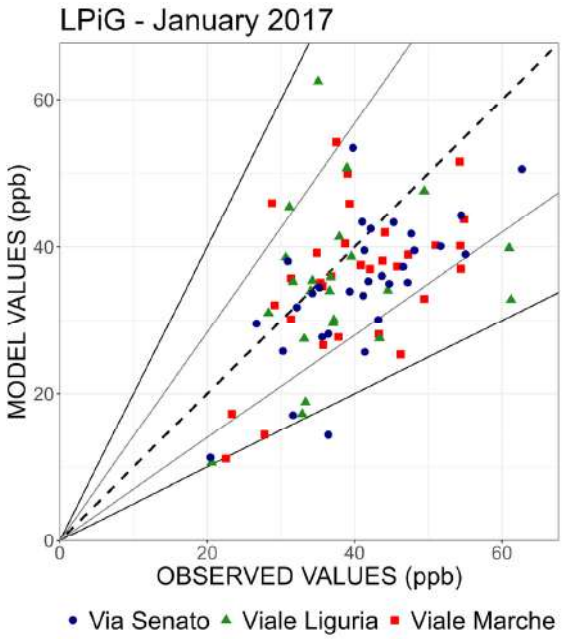

Figure 11. Scatter plot of Observed vs. Modelled NO_2 daily mean concentrations at the AQ site of Viale Marche (S1), Viale Liguria (S2), and Via Senato (S3). The dashed line has a slope of 1, the black lines have a slope of 2 and 0.5, and the grey lines have a slope of 0.7 and 1.42.

Table 3. CAMx-LPiG evaluation for the daily mean NO_2 concentrations in January 2017 (MB: mean bias; RMSE: root mean square error; NMB: normalized mean bias; COR: correlation coefficient; IOA: index of agreement).

Site	Data Coverage	Monthly Mean		MB	RMSE	NMB	COR	IOA
		Observed	Modelled					
	%	ppb	ppb	ppb	ppb	%	-	-
S1	100	39.9	35.7	−4.2	10.2	−10.5	0.51	0.69
S2	74	37.7	34.7	−2.7	12.3	−8	0.30	0.53
S3	100	40.9	34.6	−6.3	9.6	−15.5	0.68	0.72

Compared to the CAMx simulation (Table S3), the slightly higher concentrations produced by CAMx-LPiG allow us to reduce the general tendency to underestimate the observations. MB decreases from −6.7 ppb to −4.2 ppb (−38%) at site S1, from −5.7 ppb to −2.7 ppb (−53%) at site S2, and from −7.3 ppb to −6.3 ppb (−14%) at site S3. As already pointed out, the lower impact of the explicit treatment of road emissions for site S3 is due to the lower traffic intensity in the LEZ that covers the city centre.

3.2.2. Hourly Concentrations

The time series of the observed and modelled NO_2 hourly concentrations in January 2017 are shown in the SM Figure S9 for the three monitoring sites. As for the daily means time series, after a good performance in the first half of the month, both model simulations tend to underestimate the observation from 14 January to 25 January. At all sites, the main discrepancy concerns the daily minimum values, while the peak concentrations are correctly estimated most of the time. The local concentration increments provided

by CAMx-LPiG improve the estimation of the first quartile (q25) and the median of the whole data distribution at all sites, and of the third quartile (q75) at sites S1 and S3. However, the quartiles remain still underestimated. Conversely, CAMx-LPiG tends to slightly overestimate the 95th percentiles (q95) of the hourly data that are better reproduced by CAMx simulation.

The values of performance indicators for the hourly NO_2 averages simulated by CAMx-LPiG for January 2017 are reported in Table 4 (data for CAMx reported in Table S4). Overall, a high number (82.4%) of model–observation pairs are within the FAC2 area, with FAC2 values ranging from 0.80 at site S2 to 0.84 at site S1. Still, in agreement with the results for the daily averages, observations are overall underestimated. The scatter plot of hourly values for CAMx-LPiG is presented in Figure 12—for all sites (a), and for each individual one (b). As expected, most of the observed-model concentration points that fall outside the FAC2 zone are due to underestimation of the observed value. Additionally, as a consequence of the higher time resolution, both COR (0.32–0.5 range) and IOA (0.54–0.65 range) are generally lower than the daily values. Compared with CAMx, we notice an improvement in the bias-related metrics (2.1% to 7.9% decrease in NMB), while there is a mild deterioration to no change in the other performance metrics.

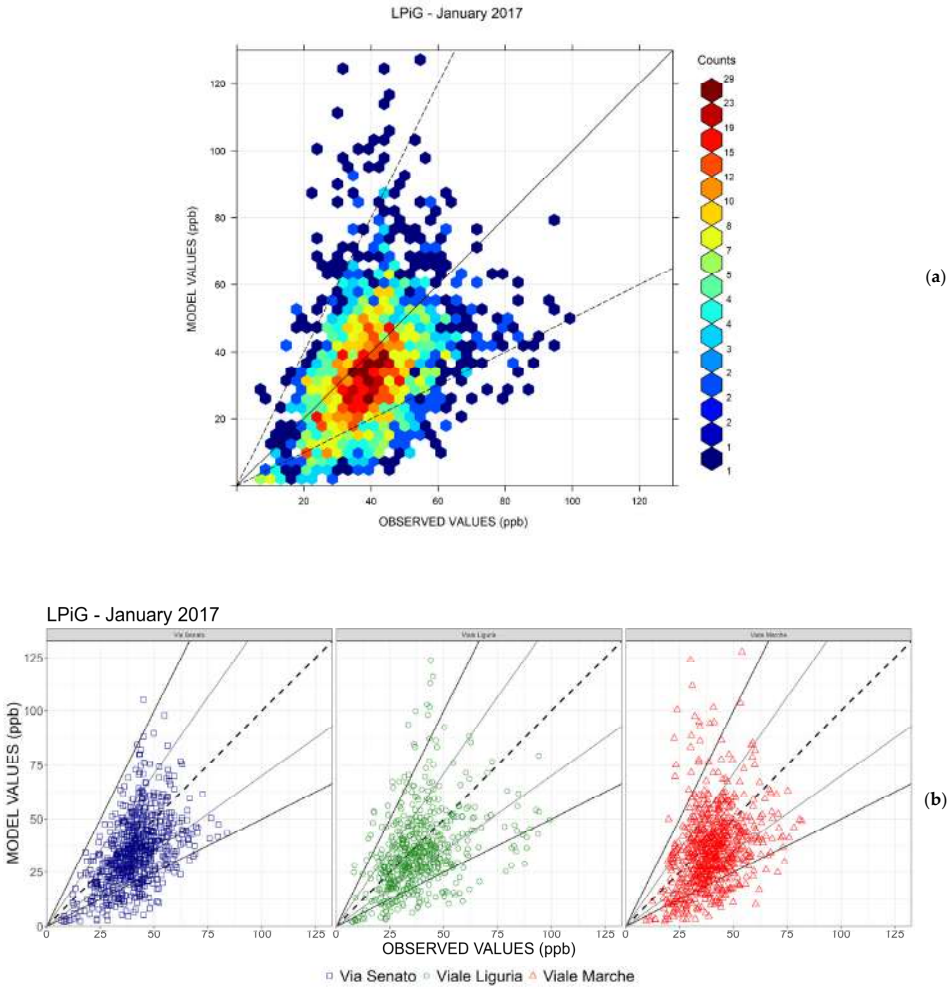

Figure 12. Panel (**a**): Openair [52] density scatterplot of the Observed vs. Modelled NO_2 hourly concentrations at all sites. The plot also shows the line with slope 1 and with dashed lines the lines with slopes of 0.5 and 2. Panel (**b**): scatterplot of the Observed vs. Modelled NO_2 hourly concentrations at the AQ site of Viale Marche (S1), Viale Liguria (S2), and Via Senato (S3). The dashed line has a slope of 1, the black lines have a slope of 2 and 0.5, and the grey lines have a slope of 0.7 and 1.42.

Table 4. CAMx-LPiG evaluation for the hourly mean NO_2 concentrations in January 2017 (MB: mean bias; RMSE: root mean square error; NMB: normalized mean bias; COR: correlation coefficient; IOA: index of agreement).

Site	Data Coverage	Hourly Mean		MB	RMSE	NMB	COR	IOA
		Observed	Modelled					
	%	ppb	ppb	ppb	ppb	%	-	-
S1	100	39.9	35.7	−4.2	18.6	−10.5	0.32	0.54
S2	75	38.3	34.8	−3.4	19.2	−9	0.38	0.60
S3	100	40.9	34.6	−6.3	15.7	−15.5	0.5	0.65

Despite the rather low correlation, the model quality objective (MQO), as defined in the FAIRMODE's report on model quality objectives [53], is satisfied for all three sites (Figure 13). The target plot for the hourly values, developed by the FAIRMODE group for the validation tool DELTA, puts in evidence the goodness of model results (MQI < 1 at all sites) and the reasons for the difficulties of the model in reproducing the observed concentration, essentially related to the low correlation and negative bias. We also tested the FAIRMODE target plot for PM_{10} and $PM_{2.5}$ at S3, the lone traffic stations with PM measurements in the LPiG study area. Both PM_{10} (MQI = 0.874) and $PM_{2.5}$ (MQI = 0.66) pass the FAIRMODE MQO. The data are presented in SM Figure S10.

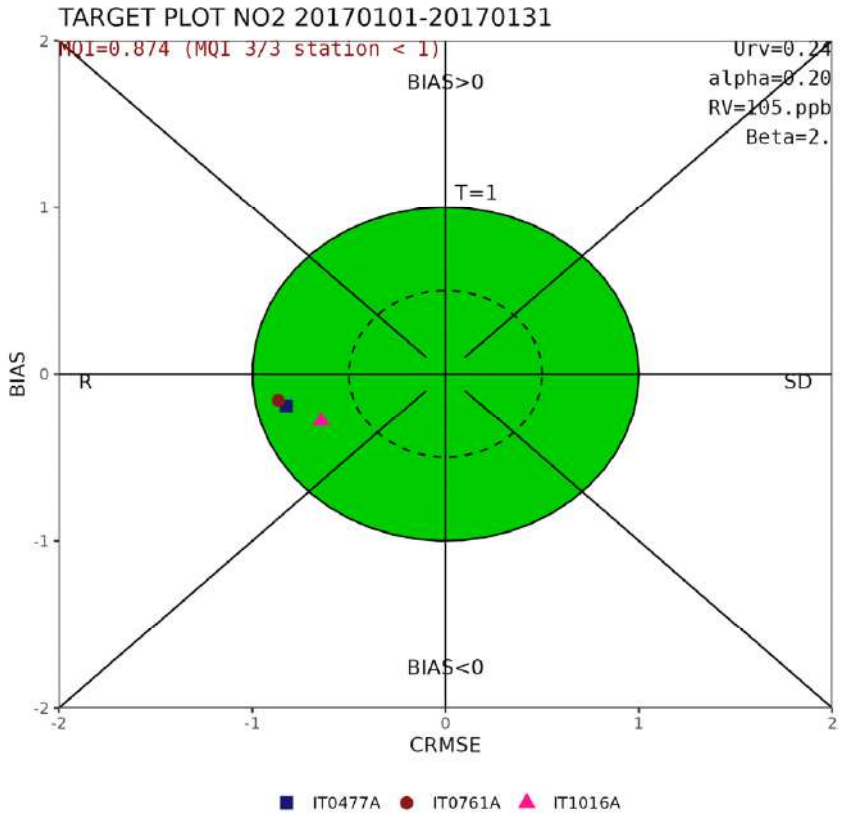

Figure 13. FAIRMODE target plot for the hourly NO_2 concentration at the three monitoring sites in January 2017. The location of the site markers explains whether model error is dominated by bias, correlation, or standard deviation.

However, model performance is strongly variable during the day, as shown in Figure 14, where the modelled and observed hourly time series at the three monitoring sites are plotted for the mean day of January. Even though the time pattern is acceptably reproduced, the model results underestimate the observed concentration during night-time

and in the central part of the day at all sites. In the first hours of the night, the negative bias is up to 20 ppb, in the early afternoon around 15 ppb, and in the late evening about 10 ppb. Conversely, observations are overestimated during morning rush hours at sites S1 and S2, and on evening rush hours at all sites. The positive bias, about 10–15 ppb, is already particularly evident in CAMx simulation for sites S1 and S3 and becomes more relevant when the increments of CAMx-LPiG are accounted for, especially at site S1.

As for the daily concentrations, CAMx-LPiG provides higher concentrations than CAMx following an hourly pattern, common at the three sites, that mirrors traffic intensity in the urban area. However, the difference between the estimated concentrations depends on the traffic exposure of the monitoring sites: differences are larger at the sites located on the outer ring road (S1, S2), namely during rush hours, and very small for most of the day at site S3 in the Low Emission Zone. With respect to the standard CAMx results, the CAMx-LPiG increments are practically negligible from midnight to 5:00 at all sites (maximum hourly mean increase of 1.1 ppb at site S2) when road emissions are very low (see Section 4). Then, together with the increase in traffic the increment rises to an early morning maximum at 7 AM of 4.9 ppb at site S2 and 3.4 ppb at site S1; for site S3 the maximum morning increase is in the same orders (2.1 ppb) but is estimated at 9:00. In the morning and afternoon, the departures between model results remain of small significance, probably due to the predominant role of vertical dispersion on both scales. Finally, during the evening rush hour, differences between the two models rise again up to greater values than in the morning peak. Maximum CAMx-LPiG evening increments are 6.6 ppb at site S1 at 7 PM, 7.1 ppb at site S2 at 7 PM, and 1.8 ppb at site S3 at 7 PM, however, at all sites differences persist for all the evening hours and decline only after 9 PM. The boxplots for the hourly increments of CAMx-LPiG compared to CAMx are presented in Figure S11.

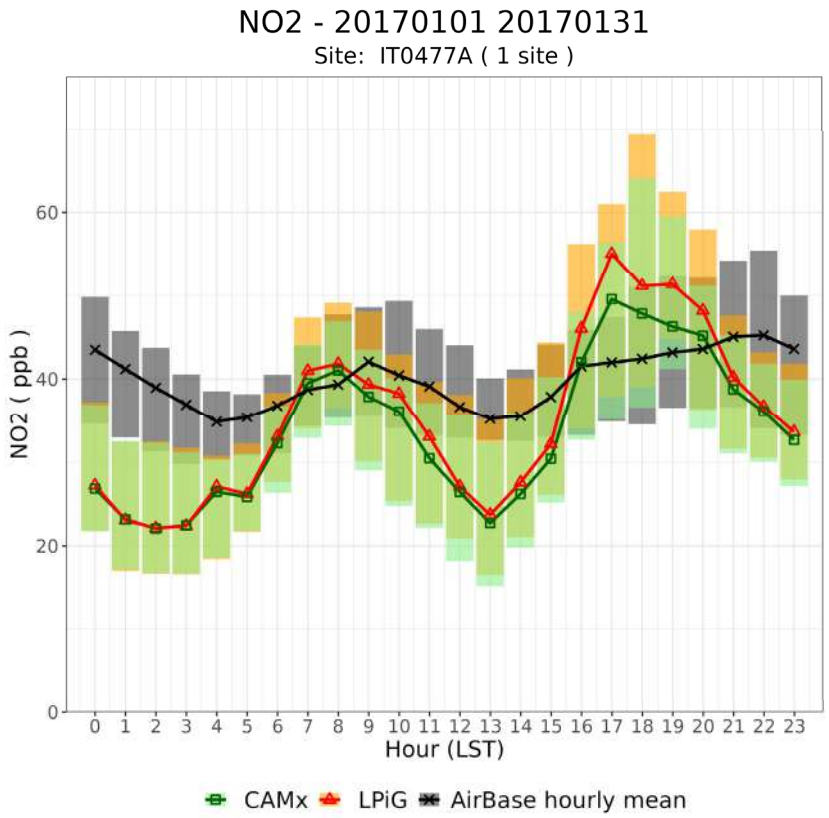

Figure 14. *Cont.*

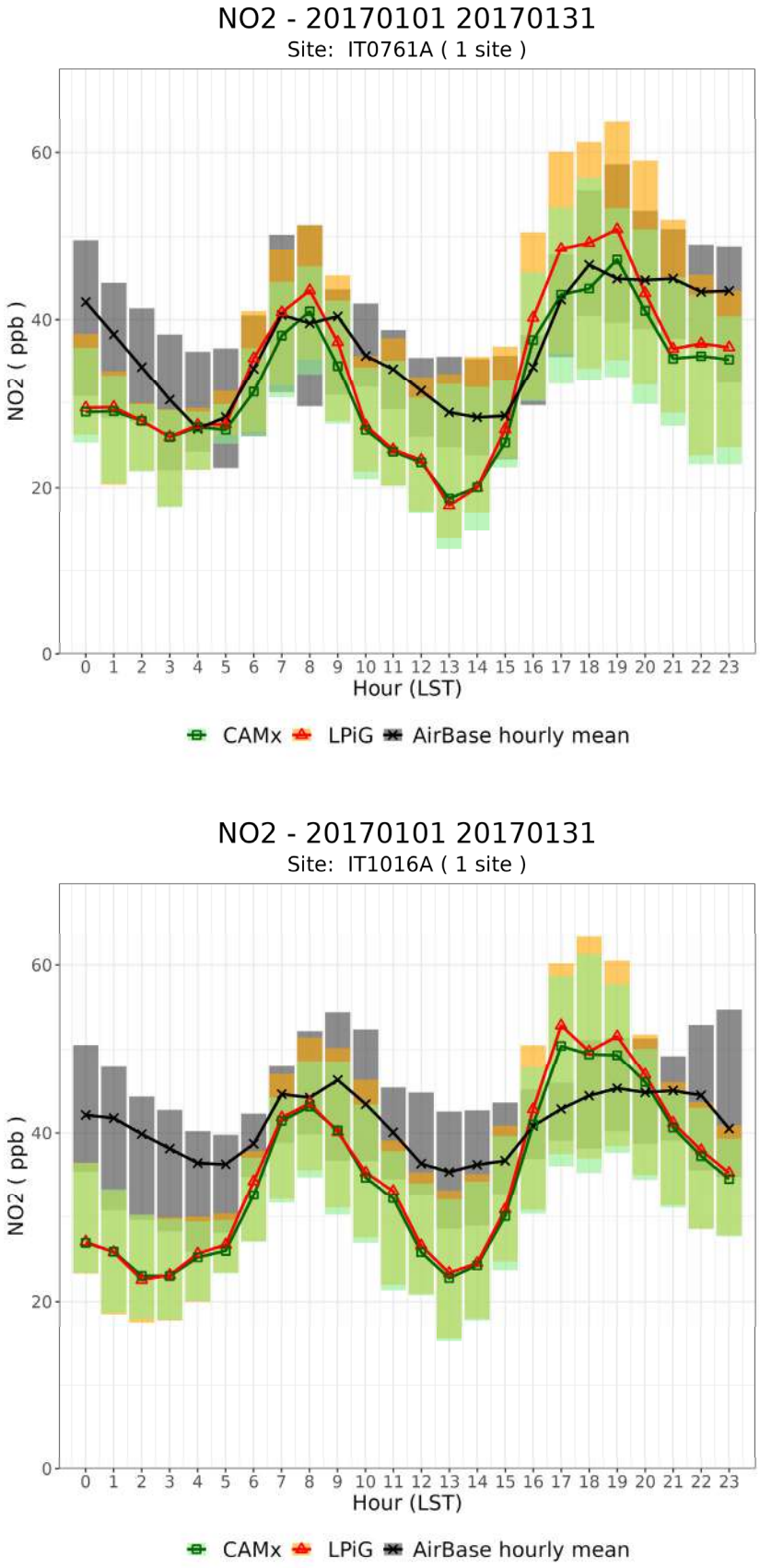

Figure 14. Hourly NO_2 concentration time series for the AQ stations of Viale Marche (S1: IT0477A), Viale Liguria (S2: IT0761A) and Via Senato (S3: IT1016A) for January 2017. The black line represents the observed value, the red line represents the CAMx-LPiG simulation, and the green line represents the CAMx simulation. The boxes' top and bottom values are the first and third quartiles.

4. Discussion

In Section 3.1 we presented the cross-road profiles of NO_2 concentration increments estimated by the hybrid model CAMx-LPiG. While such increments can help to close the gap between model predictions and observations (i.e., partially reducing the mean bias absolute value), an ad hoc validation of such increments cannot be carried out using the current observation network. A possible approach to this problem is the comparison of the simulated increments to the results of measurement campaigns aimed to understand the influence of traffic pollution on near road air quality. The results of two meta-analyses on those studies showed that most of the decay in NO_2 concentration happens in the first 200–500 m before reaching background values in a gradual way [54,55]. Karner et al. 2010 found an increase in edge of the road measurements with respect to background concentration of 42% [54]. Comparing these results with the cross-road increments of Figure 9, CAMx-LPiG showed a limited increase compared to concentration at 250 m from the roadside (mean increase of circa 5% with few values exceeding 10%). While this comparison provides valuable insights into the performance of CAMx-LPiG in simulating road traffic-related effects on air quality, it is important to consider the differences between the experimental studies underlying the two meta-analyses and the modeling results. First, most of the studies cited in the two meta-analyses are based on motorways/highways' impacts on air quality rather than urban roads. Furthermore, most of the data come from the daytime measurements campaign [54], while the data from this study are a mean for the month of January. Keeping in mind the inherent differences between LPiG and the considered datasets, the comparison points out that CAMx-LPiG shows a smoother transect concentration with respect to the literature's data. Possible reasons for such difference could be: (a) the overestimation of the puff horizontal and vertical dispersion due to the absence, in this first version of CAMx-LPiG, of the treatment of the urban canopy; (b) the sampling resolution of the Gaussian concentration function set to 50 m, due to computational limitations. It is worth noting that, although the puff dispersion is probably overestimated, the total modelled concentration shows a moderate-to-low negative bias, which could be related to overall good performance of the CAMx model at the urban scale, whose contribution is particularly relevant also at traffic receptor [5]. In some cases, the CAMx model may slightly overestimate the contributions from surrounding sources other than road sources. Also, the latter effect can be ascribed to the absence of the urban canopy.

The evaluation of the daily concentrations showed a prolonged period of underestimation in the second half of the month. To understand the possible reasons for the underestimation, in Figure 15 we propose a brief validation of the WRF meteorological data for the city of Milan.

The position of the meteorological stations used in the validation is shown in Figure S12. The validation shows good performance for the water vapour mixing ratio, with a high correlation coefficient and IOA and low mean bias. The temperature is underestimated by the WRF model, but it presents a good correlation score. Precipitation is poorly reproduced, but it does not play a key role during the considered period. The most important meteorological parameter to investigate is wind speed. As shown in Figure 15, model and observation are generally well aligned during the first decade of the month. Conversely, from the 13–26 January the meteorological model systematically overestimates the observed wind speed and reproduces some events of strong wind that do not occur in the measured data. This period coincides with the underestimation of NO_2 concentrations. It is worth noting that wind speed overestimation takes place when observed wind speed shows extremely low values that are generally not captured by meteorological models. Moreover, the WRF model shows clear discrepancies in reproducing both temperature and mixing ratio in the same period. The overall analysis of the meteorological performance

indicates that WRF is not able to capture the strong stagnant conditions taking place from the 13–26 January. Further investigations are needed to understand whether the observed discrepancies in concentration values are related to the incorrect reconstruction of the meteorological conditions over the whole airshed or they are also related to the absence of local scale information on the urban canopy, such as building heights and street canyons, that could play a more relevant role on atmospheric dispersion during stagnant conditions.

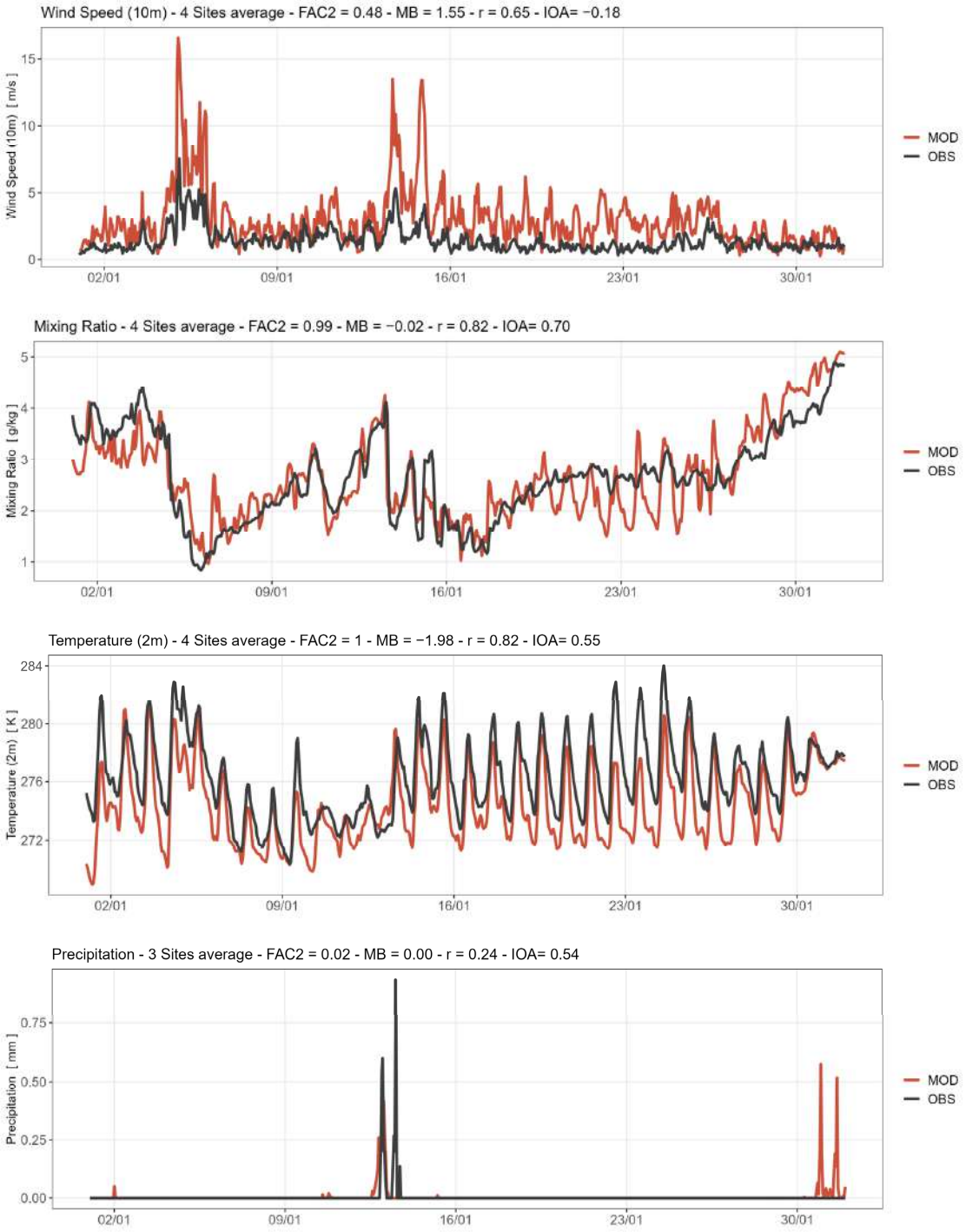

Figure 15. Validation of hourly meteorological fields (Wind Speed, Water Vapor Mixing Ratio, Temperature and Precipitation) at the available meteorological stations of Milan city centre. Observations are depicted in black (OBS) while model values are depicted in red (MOD). Statistical parameters are reported in the figures (FAC2: Factor of two, MB: Mean Bias, r: Pearson's correlation coefficient, and IOA: Index of Agreement).

Finally, another aspect to be improved is the reproduction of the daily concentration profile. The mean day profile of the simulated NO_2 concentration differs from the observed one, especially during night-time conditions and in the central hours of the day at all sites (Figure 14). The temporal emission profile and meteorological conditions are the two main factors affecting the diurnal concentration profile. As for the former, the daily evolution of the NOx emission rate at the corresponding model cells of the three monitoring stations is shown in Figure 16.

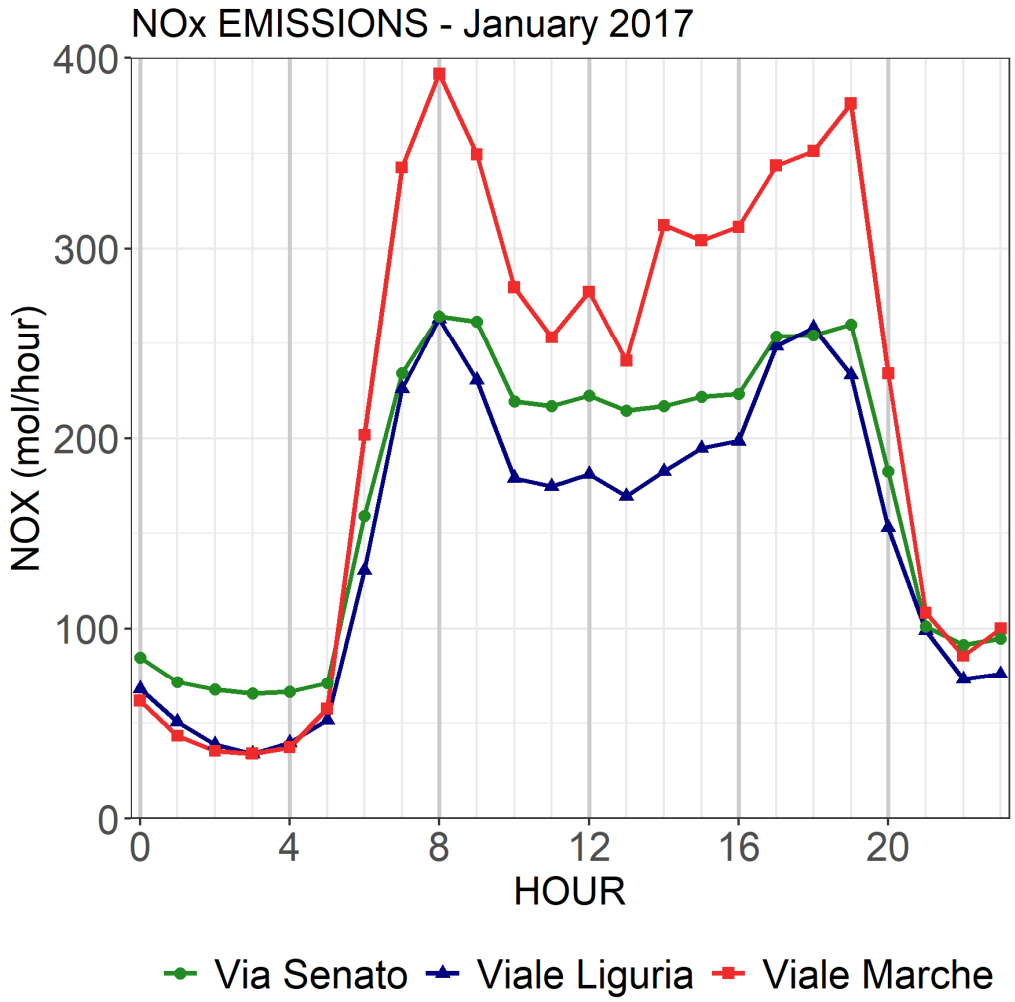

Figure 16. Hourly variation of NOx emissions at the three monitoring stations: Viale Marche (S1, red), Viale Liguria (S2, blue), and Via Senato (S3, green).

The NOX emission profile, which is based on observed traffic data, presents a very reasonable trend with two rush hour peaks, at 08:00 and 18:00/19:00. This trend is shown also by the observed and modelled hourly concentration profiles presented in Section 3.2.2 (Figure 14). The period at which peak concentration is reached for both morning and evening rush hours for S2 and S3 is generally well modelled, though partially overestimated during the afternoon period. Differently, while measured concentrations tend to remain stable for most of the night-time, modelled concentrations sharply decline after 19:00 to a night-time minimum. Furthermore, the midday decline is more accentuated in the modelled concentrations than in observed values. The midday underestimation could be driven by the development of the Planet Boundary Layer (PBL) height during daytime (Figure 17). In PiG, and therefore also in LPiG, the puff growth along the vertical dimension is due to vertical turbulence and is capped by the PBL height, hence an overestimation of the vertical dispersion can strongly affect the LPiG simulated concentrations at ground level.

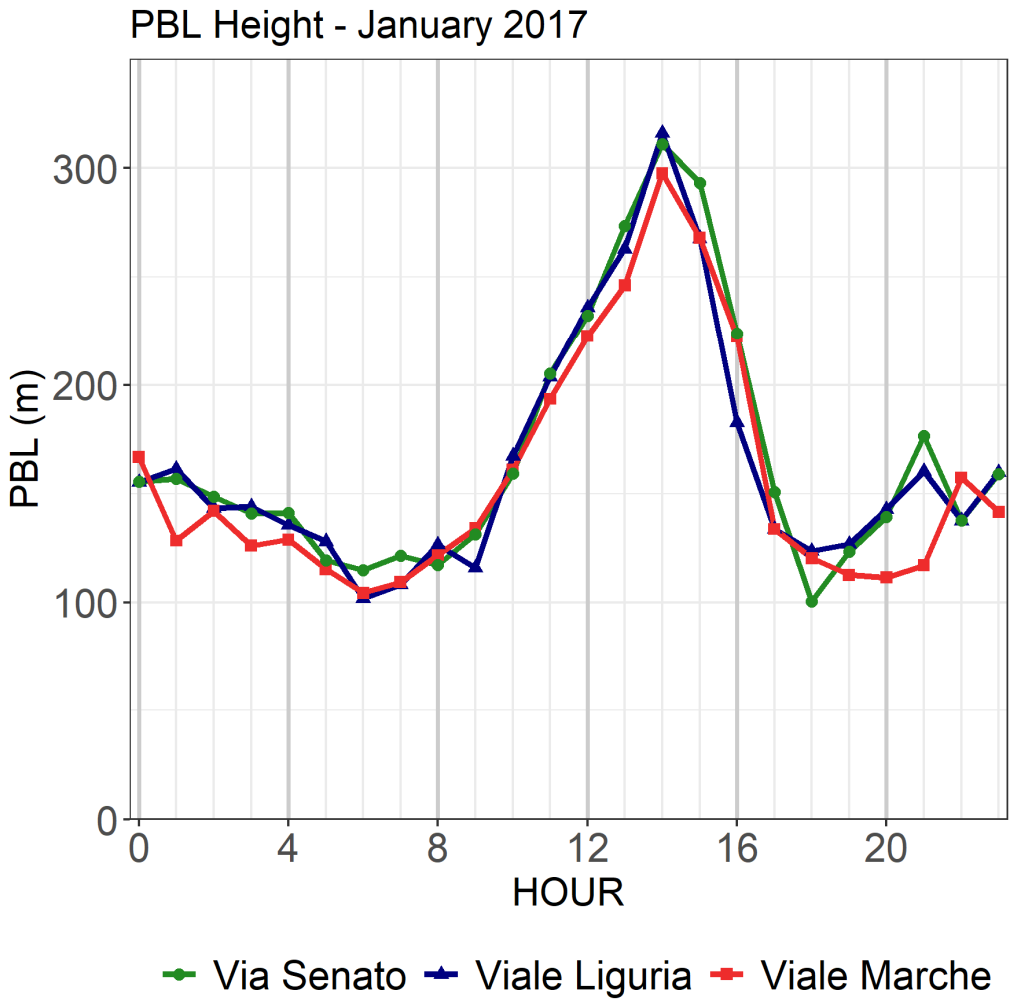

Figure 17. Hourly variation of PBL height at the three monitoring stations: Viale Marche (S1, red), Viale Liguria (S2, blue), and Via Senato (S3, green) in January 2017.

The PBL diurnal profiles at the three monitoring stations are shown in Figure 17. As expected, the PBL increases after sunrise (around 8:00 CET in January for Milan) and decreases to a minimum after sunset (around 17:00 CET in January for Milan). The midday underestimation of NO_2 coincides in time with the maximum PBL values (14:00 CET), suggesting that the CAMx negative bias could be related to an overestimation of the maximum PBL height during daytime. Differently, during afternoon hours the model overestimates the observed values. NO_2 overestimation is probably caused by a corresponding overestimation of NOx concentrations (see as an example Figure S16) due to a too sharp decrease of PBL depth during afternoon hours. Finally, during night-time hours, CAMx-LPiG shows a clear underestimation of both NOx and NO_2 that can be ascribed to an excess of dilution during evening and night hours. The obtained results confirm that the reconstruction of the meteorological fields at the urban scale and their effects on pollutant dispersion need to be improved to better reproduce the atmospheric fate of the pollutant emissions at both urban and local scales.

5. Conclusions

This paper presents the CAMx-LPiG (Comprehensive Air Quality Model with Extensions—Linear Plume in Grid) online hybrid model, combining the CAMx Chemistry and Transport Model (CTM) with a sub-grid module for simulating road traffic emissions. The LPiG module, developed in CAMx 7.1, introduces key modifications to the initial

puff shape, sampling equation, emission release time, and puff lifetime. The use of a fine sampling grid for the puff module concentration results in a better reproduction of the spatial concentration gradients of modelled pollutants with respect to the stand-alone CAMx model. The LPiG module improves road traffic pollution studies by evaluating the contribution of each road link, while the online approach avoids issues like emission double counting and enables consistent treatment of NOx/O_3 and basic PM chemistry. The structure of the LPiG inputs is the same as the original PiG module in CAMx, so as to maintain a user-friendly approach for CAMx users.

CAMx-LPiG was developed within a bottom-up modeling framework designed to simulate the impact of road transport on air quality and human health, focusing on future mobility scenarios. The hybrid module is an important development towards this goal, allowing us to investigate the spatial patterns of concentrations at a finer resolution compared to the Eulerian CAMx grid. By explicitly simulating the dispersion from single road links, it leverages the bottom-up emission estimates, rather than spreading them across the entire model cell. The high resolution of CAMx-LPiG will be essential for more accurately estimating population exposure to air pollutants, with plans to extend the model for dynamic exposure assessments at the sub-grid scale.

As a test case, CAMx-LPiG was applied to enhance the assessment of the urban traffic emission impact on air quality in the urban area of Milan, showing potential effectiveness in simulating NO_2 concentrations. Promising performances were found for a winter month, where CAMx-LPiG showed a negative bias smaller than stand-alone CAMx at urban traffic monitoring stations. However, the concentration increments provided by CAMx-LPiG are still not enough to fill the gap between NO_2 model predictions and observations. Even though the comparison with other works dealing with near-road dispersion of traffic emissions is to be taken with caution, it appears that the effects of road traffic might be underestimated by CAMx-LPiG. Furthermore, the effect of the urban canopy, currently neglected, looks like a crucial factor in improving both the reconstruction of the meteorological fields and the local atmospheric dispersion simulated by the hybrid component LPiG.

The lack of specific treatment for meteorology and puff dispersion inside the urban canopy and street canyons is one of the main limitations of the current version of the model and future works are already planned to improve CAMx-LPiG. Furthermore, another aspect that can be improved upon is the initial dispersion by including traffic specific turbulent dispersion coefficients (sigma) that consider vehicle induced turbulence. Additionally, the chemical evolution of puffs could be better addressed in order to improve the performance of LPiG module. We selected the GREASD option, originally designed for large NOx plumes and focusing on inorganic gas-phase reactions. This option includes twenty-three NOx/O_3 reactions, which we assumed are valid for traffic puffs' early life. However, ongoing tests with the full gas chemistry option aim to validate this assumption. Finally, the last limitations are related to the concurrent consumption of background ozone of overlapping puffs. When multiple puffs overlap with each other an excessive consumption of background ozone can occur, leading to unrealistic ozone and NO_2 concentrations. The original PiG has a feature to treat overlapping puffs that will be tested to be extended also to linear sources in LPiG.

In conclusion, CAMx-LPiG appears to be a valuable tool for evaluating road traffic emissions across multiple scales, from the regional to the city level, and identifying pollution hotspots. Its versatility makes it effective for analyzing the impact of mobility policies at different scales, including the transition to electric mobility. Future model developments will enhance the simulation of urban-scale meteorological processes, improving air quality modeling at the street level.

Supplementary Materials: The following supporting information can be downloaded at: https://www.mdpi.com/article/10.3390/atmos16050604/s1, Section S1: Additional information on the setting of the puff's initial conditions; Figure S1: Definition of the puff geometry in case of wind direction normal to the street segment; Figure S2: Definition of the puff geometry in case of wind direction parallel to the street segment; Section S2: Additional information on the Super Gaussian Sampling; Table S1: Polynomial fit equation for the value of Py for the different road length classes; Figure S3: Polynomial fit for the value of Py for different road length classes; Figure S4: Equation for the correction coefficients for the Super Gaussian sampling; Section S3: Test case results for the modified emission timestep; Figure S5: Left panel: Mean January 2010 concentration for a test case in the city center of Milan, right panel: Relative difference between the two methods of emitting the puffs; Figure S6: Simulated roads and CTM grid used in the sensitivity tests of this section; Table S2: Comparison of the computational time needed to simulate one day of LPiG with different number of road links; Section S4: Tables and Figures in support to the model validation of Chapter 3; Table S3: CAMx validation for daily NO_2 values for the month of January 2017; Figure S7: Daily NOx modeled concentration time series for the AQ stations of Viale Marche (IT0477A), Viale Liguria (IT0761A) and Via Senato (IT1016A) for January 2017; Figure S8: Scatter plot of Observed vs Modelled NO_2 daily mean concentrations at the AQ site of Viale Marche, Viale Liguria and Via Senato for the CAMx simulation; Figure S9: Time series of hourly NO2 concentrations at the AQ stations of Viale Marche (Site S1: IT0477A), Viale Liguria (Site S2: IT0761A) and Via Senato (Site S3: IT1016A) in January 2017. (Black line: observed values; red line: CAMx-LPiG simulation; green line: CAMx simulation);Table S4: CAMx validation for hourly NO_2 values for the month of January 2017; Figure S10: FAIRMODE target plot for PM10 and PM2.5; Figure S11: Hourly boxplot of NO_2 difference in concentration between CAMx-LPiG and CAMx simulation for the AQ stations of Viale Marche (S1: IT0477A), Viale Liguria (S2: IT0761A) and Via Senato (S3: IT1016A) for January 2017; Figure S12: Daily time series of NOx and NO2/NOx ratio for the traffic monitoring stations of Milan (S1, S2, and S3 of the main text) and at the urban background station for Milano Pascal (UB in the figure); Section S5: Figure in support to the discussion of Chapter 4; Figure S13: Location of the meteorological monitoring stations used in the validation of the WRF simulation; Section S6: NOx validation for UT traffic station of Piazza Zavattari; Figure S14: Location of AQ station of Piazza Zavattari (red triangle) and AREAC Low emission Zone (green); Figure S15: Daily NOx concentration time series for the AQ stations of Piazza Zavattari (MI503) for January 2017; Figure S16: Hourly NOx concentration time series for the AQ stations of Piazza Zavattari (MI503) for January 2017; Table S5: CAMx LPiG and CAMx validation for daily NOx values for the month of January 2017.

Author Contributions: Conceptualization, A.P., V.A. and G.P.; methodology, A.P., V.A., G.L. and G.P.; software, A.P.; supervision, G.L. and G.P.; visualization, A.P.; writing—original draft, A.P. and V.A.; writing—review and editing, A.P., V.A., G.L. and G.P. All authors have read and agreed to the published version of the manuscript.

Funding: This work has been financed by the Research Fund for the Italian Electrical System under the Three-Year Research Plan 2022–2024 (DM MITE n. 337, 15.09.2022), in compliance with the Decree of 16 April 2018.

Institutional Review Board Statement: Not applicable.

Informed Consent Statement: Not applicable.

Data Availability Statement: CAMx-LPiG is an original modification of the original CAMx software version 7.1 and is written in FORTRAN. The new code includes new routines and modifications to existing ones. Since the LPiG module is integrated into CAMx, the model is designed to work in Unix/Linux environments. The source code for CAMx-LPiG is publicly available via Zenodo (https://doi.org/10.5281/zenodo.14944768). The code is distributed under the original CAMx license and the GNU lesser general public license for the new LPiG material.

Conflicts of Interest: The authors declare no conflicts of interest. The funders had no role in the design of the study; in the collection, analyses, or interpretation of data; in the writing of the manuscript; or in the decision to publish the results.

Appendix A

Mean Bias (MB)

$$MB = \frac{1}{N}\sum_{t=0}^{N}(M_t - O_t)$$

Normalized Mean Bias (NMB)

$$NMB = \frac{1}{N}\frac{\sum_{t=0}^{N}(M_t - O_t)}{\sum_{t=0}^{N}O_t} \times 100\%$$

Index of Agreement (IOA)

$$IOA = 1 - \frac{\sum_{t=0}^{N}(M_t - O_t)^2}{\sum_{t=0}^{N}\left(\left|M_t - \overline{O}\right| + \left|M_t - \overline{O}\right|\right)^2}$$

Root Mean Square Error (RMSE)

$$RMSE = \sqrt{\frac{1}{N}\sum_{t=0}^{N}(M_t - O_t)^2}$$

Correlation (COR)

$$r = \frac{\sum_{t=0}^{N}\left(M_t - \overline{M}\right)\cdot\left(O_t - \overline{O}\right)}{\sqrt{\sum_{t=0}^{N}\left(M_t - \overline{M}\right)^2}\cdot\sqrt{\sum_{t=0}^{N}\left(O_t - \overline{O}\right)^2}}$$

where:

M_t = modelled concentration at time t (upper line indicates mean variable for all period)
O_t = observed concentration at time t (upper line indicates mean variable for all period)
N = number of cases.

Appendix B LPiG Emission Timestep

In the original PiG sub-model, a puff is emitted for every source at the timestep of the finest computational domain used for CAMx simulation. When working with fine grids (i.e., 1 km), the emission timestep is often lower than a minute, thus generating a high number of puffs that slow down the execution of the model. To reduce the computational time needed to simulate a high number of road links (e.g., the network of primary roads in a city centre), LPiG limits the number of emitted puffs from linear sources to one puff every 10 min circa, that is six or seven synpuffs per hour. The exact number of puffs depends on the computational time step (sec) of the master grid of the Eulerian model. At the beginning of each hour, the number of puffs emitted from each linear source (N_{Puffs}) is computed as:

$$N_{Puffs} = CEILING\left(\frac{3600}{dt_{LPiG}}\right)) \quad \text{(A1)}$$

where CEILING is the Fortran function that returns the least integer greater than or equal to the argument passed to the function and dt_{LPiG} (sec) is the emission time step of the LPiG sources and is equal to:

$$dt_{lpig} = NINT\left(\frac{600}{dt_{CAMX}}\right) \cdot dt_{CAMX} \quad \text{(A2)}$$

where dt_{CAMX} (sec) is the master grid time step and NINT is the Fortran function that rounds its argument to the nearest whole number.

For the last puff of the hour, the emission timestep needs to be recomputed to prevent the total emission time from exceeding the hour, which would lead to emitting more pollutants mass than needed. The last time step is equal to:

$$dt_{LPiG,N_{Puffs}} = 3600 - \left(dt_{LPiG} \cdot (N_{puffs} - 1)\right) \quad \text{(A3)}$$

Considering that LPiG can be applied with a CAMx setup adopting an arbitrary number of nested domains, the following assumptions are made during the puff emission and life:

- The initial age of the leading point of the puff is equal to the computational time step of the grid in which the puff is emitted and not to dt_{LPiG}
- The puff is not divided into multiple puffs if the emission time exceeds the specific maximum timestep or if its dimension exceeds half of the finest grid cell.
- The puff evolution (chemistry, diffusion and advection) is not modified, the puff is free to evolve with the timestep of the grid where it is located.

The updates to the puff emission timestep described in this paragraph allowed us to reduce the computational burden of CAMx LPiG, with negligible differences from the original PiG formulation for the emission timestep. In Supplementary Materials Section S3, a brief test case highlighting the differences between the original PiG emission timestep and the modified one is presented. For this test case, the maximum difference in concentrations does not exceed 1.5%, with a decrease in computational time of 77%.

Appendix C GREASD Chemistry Modifications

As previously stated, the LPiG code can work with both the chemistry options available in PiG. The IRON PiG mechanism can solve all the equations for gas phase reactions according to the chemical schemes available in CAMx (i.e., CB05, CB06, SAPRC7), but the computational time strongly increases with the number of roads processed by LPiG. Moreover, with the IRON PiG option, all particulate matter must be considered inert, thus excluding all secondary PM from the simulations. To solve these issues CAMx developers introduced the GREASD PiG option. The GREASD PiG mechanism was developed to treat the early stages of large point stack plumes dispersion and includes 23 mainly inorganic reactions for NOx/O3 chemistry. The complete chemistry that includes VOC reactions is dealt with later at the grid scale by the Eulerian model when the plumes have reached their final stage [56]. Considering that many available hybrid and local scale models implement a simplified chemistry scheme when dealing with road traffic plumes, which can start from simple photo stationary reactions set up to more complex reaction sets that closely resemble the GREASD reaction sets [18,22,57,58], we consider the photochemical reactions included in the GREASD option to be valid also for the early stages of road traffic plumes handled by LPiG. However, the GREASD chemical option of PiG cannot be used "as is" for LPiG sources. In GREASD PiG, puffs are dumped to the CAMx grid when they reach the last stage of puff life when organic chemistry starts to play an important role in the puff chemistry [34].

However, this condition is valid only for power plant plumes and leads to a too short lifetime of road traffic plumes (about 1 min). Therefore, for LPiG sources the life of the puff does not end when the previous condition is met. A maximum life span for the puff

is set equal to the puff emission time step (dt_{LPiG}). This condition allows us to capture the sub-grid spatial concentration gradient due to the linear sources while limiting the computational burden that would arise from having many active puffs on the grid. Lastly, the maximum puff life span condition allows only one puff to be active for each road link, thus reducing the overlap between puffs which can lead to concurrent consumption of background ozone from multiple puffs.

Appendix D

The structure of the CAMx input files for point emission is valid also for linear sources, even if some of the variables have a different meaning, due to the 2-dimensional features of line sources. Particularly:

- The sign of variable dstk (stack diameter in original CAMx point sources file) allows point/linear sources that are handled by the sub-grid schemes PiG/LPiG (dstk < 0) to be distinguished from point sources that are handled only at the grid level (dstk $\geq$ 0). The absolute value of the variable dstk in CAMx-LPiG represents the average width of the road segment, while in PiG it represents the stack diameter of the point source.
- The sign of variable hstk (stack height in the original CAMx point sources file) allows point sources (hstk $\geq$ 0) to be distinguished from linear sources (hstk < 0). In CAMx-LPiG, the emission height is not read from hstk but is replaced by the effective emission height, assumed equal to 2 m, as in ADMS-local, a gaussian model for urban air quality [36].
- In the original CAMx point source file, the xstk and ystk variables are the horizontal coordinates of the barycenter of the stack, whereas, variables tstk and vstk are the temperature and the exit velocity (in vertical direction) of the emission at the stack, respectively. For linear sources, xstk and ystk represent the horizontal coordinates of one vertex of the road segment (i.e., xA, yA), and tstk and vstk are used for the horizontal coordinates of the other vertex (i.e., xD, yD); the emission temperature is set to 373 K [59], and the vertical component of the emission velocity is set to 0.1 m/s.

The differences between the PiG and LPiG variables are summarized in Table A1. Units of measurements of the emissions in input to LPiG also follow the CAMx-PiG convention (mol/h for gasses and g/h for PM species).

Table A1. PiG and LPiG input variables meaning.

PiG		LPiG		Notes
xstk	X coordinate	xa	X coordinate of the first street vertex.	
ystk	Y coordinate	ya	Y coordinate of the first street vertex.	
hstk	Stack height	LPiG_f	LPiG Flag.	If hstk < 0 the source is treated with LPiG.
tstk	Temperature	xb	X coordinate of the second street vertex.	
vstk	Exit velocity	Yb	Y coordinate of the second street vertex.	
dstk	Stack diameter	Ws	Road width.	If dstk < 0 the source is treated with a sub-grid module (PiG/LPiG)

References

1. United Nations Department of Economic and Social Affairs Population Division. *World Urbanization Prospects The 2018 Revision*; United Nations: New York, NY, USA, 2019.
2. EEA. *Air Quality in Europe—2020 Report*; European Environment Agency: Copenhagen, Denmark, 2020; ISBN 1977-8449.
3. World Health Organization. *WHO Global Air Quality Guidelines: Particulate Matter (PM2.5 and PM10), Ozone, Nitrogen Dioxide, Sulfur Dioxide and Carbon Monoxide*; World Health Organization: Geneva, Switzerland, 2021.
4. EEA. *Air Quality in Europe 2022. Report No. 05/2022*; European Environmental Agency: Copenhagen, Denmark, 2022.
5. Pepe, N.; Pirovano, G.; Balzarini, A.; Toppetti, A.; Riva, G.M.; Amato, F.; Lonati, G. Enhanced CAMx Source Apportionment Analysis at an Urban Receptor in Milan Based on Source Categories and Emission Regions. *Atmos. Environ. X* **2019**, *2*, 100020. [CrossRef]

6. EC: Communication from the Commission. *The European Green Deal*; European Commission: Luxembourg, 2019.
7. European Commission. *Motorways*; European Commission, Directorate General for Transport: Brussels, Belgium, 2018.
8. Sokhi, R.S.; Moussiopoulos, N.; Baklanov, A.; Bartzis, J.; Coll, I.; Finardi, S.; Friedrich, R.; Geels, C.; Grönholm, T.; Halenka, T.; et al. Advances in Air Quality Research—Current and Emerging Challenges. *Atmos. Chem. Phys.* **2022**, *22*, 4615–4703. [CrossRef]
9. Jensen, S.S.; Ketzel, M.; Becker, T.; Christensen, J.; Brandt, J.; Plejdrup, M.; Winther, M.; Nielsen, O.K.; Hertel, O.; Ellermann, T. High Resolution Multi-Scale Air Quality Modelling for All Streets in Denmark. *Transp. Res. Part D Transp. Environ.* **2017**, *52*, 322–339. [CrossRef]
10. Kumar, A.; Patil, R.S.; Dikshit, A.K.; Kumar, R.; Brandt, J.; Hertel, O. Assessment of Impact of Unaccounted Emission on Ambient Concentration Using DEHM and AERMOD in Combination with WRF. *Atmos. Environ.* **2016**, *142*, 406–413. [CrossRef]
11. Lefebvre, W.; Vercauteren, J.; Schrooten, L.; Janssen, S.; Degraeuwe, B.; Maenhaut, W.; de Vlieger, I.; Vankerkom, J.; Cosemans, G.; Mensink, C.; et al. Validation of the MIMOSA-AURORA-IFDM Model Chain for Policy Support: Modeling Concentrations of Elemental Carbon in Flanders. *Atmos. Environ.* **2011**, *45*, 6705–6713. [CrossRef]
12. Oh, I.; Hwang, M.K.; Bang, J.H.; Yang, W.; Kim, S.; Lee, K.; Seo, S.C.; Lee, J.; Kim, Y. Comparison of Different Hybrid Modeling Methods to Estimate Intraurban NO2 Concentrations. *Atmos. Environ.* **2021**, *244*, 117907. [CrossRef]
13. Fernandes, A.P.; Rafael, S.; Lopes, D.; Coelho, S.; Borrego, C.; Lopes, M. The Air Pollution Modelling System URBAIR: How to Use a Gaussian Model to Accomplish High Spatial and Temporal Resolutions. *Air Qual. Atmos. Health* **2021**, *14*, 1969–1988. [CrossRef]
14. Hooyberghs, H.; De Craemer, S.; Lefebvre, W.; Vranckx, S.; Maiheu, B.; Trimpeneers, E.; Vanpoucke, C.; Janssen, S.; Meysman, F.J.R.; Fierens, F. Validation and Optimization of the ATMO-Street Air Quality Model Chain by Means of a Large-Scale Citizen-Science Dataset. *Atmos. Environ.* **2022**, *272*, 118946. [CrossRef]
15. Fu, X.; Xiang, S.; Liu, Y.; Liu, J.; Yu, J.; Mauzerall, D.L.; Tao, S. High-Resolution Simulation of Local Traffic-Related NOx Dispersion and Distribution in a Complex Urban Terrain. *Environ. Pollut.* **2020**, *263*, 114390. [CrossRef]
16. Degraeuwe, B.; Pisoni, E.; Christidis, P.; Christodoulou, A.; Thunis, P. SHERPA-City: A Web Application to Assess the Impact of Traffic Measures on NO2 Pollution in Cities. *Environ. Model. Softw.* **2021**, *135*, 104904. [CrossRef]
17. Ferrari, F.; Maffeis, G.; Flemming, J.; Gianfreda, R. UTAQ, A TOOL TO MANAGE THE SEVERE AIR POLLUTION EPISODES. *Environ. Eng. Manag. J.* **2020**, *19*, 1915–1926. [CrossRef]
18. Briant, R.; Seigneur, C. Multi-Scale Modeling of Roadway Air Quality Impacts: Development and Evaluation of a Plume-in-Grid Model. *Atmos. Environ.* **2013**, *68*, 162–173. [CrossRef]
19. Kim, Y.; Wu, Y.; Seigneur, C.; Roustan, Y. Multi-Scale Modeling of Urban Air Pollution: Development and Application of a Street-in-Grid Model (v1.0) by Coupling MUNICH (v1.0) and Polair3D (v1.8.1). *Geosci. Model Dev.* **2018**, *11*, 611–629. [CrossRef]
20. Kim, Y.; Lugon, L.; Maison, A.; Sarica, T.; Roustan, Y.; Valari, M.; Zhang, Y.; André, M.; Sartelet, K. MUNICH v2.0: A Street-Network Model Coupled with SSH-Aerosol (v1.2) for Multi-Pollutant Modelling. *Geosci. Model Dev.* **2022**, *15*, 7371–7396. [CrossRef]
21. Wang, T.; Liu, H.; Li, J.; Wang, S.; Kim, Y.; Sun, Y.; Yang, W.; Du, H.; Wang, Z.; Wang, Z. A Two-Way Coupled Regional Urban–Street Network Air Quality Model System for Beijing, China. *Geosci. Model Dev.* **2023**, *16*, 5585–5599. [CrossRef]
22. Karl, M.; Walker, S.-E.; Solberg, S.; Ramacher, M.O.P. The Eulerian Urban Dispersion Model EPISODE—Part~2: Extensions to the Source Dispersion and Photochemistry for EPISODE–CityChem v1.2 and Its Application to the City of Hamburg. *Geosci. Model Dev.* **2019**, *12*, 3357–3399. [CrossRef]
23. Wang, Y.; Ma, Y.-F.; Muñoz-Esparza, D.; Dai, J.; Li, C.W.Y.; Lichtig, P.; Tsang, R.C.-W.; Liu, C.-H.; Wang, T.; Brasseur, G.P. Coupled Mesoscale–Microscale Modeling of Air Quality in a Polluted City Using WRF-LES-Chem. *Atmos. Chem. Phys.* **2023**, *23*, 5905–5927. [CrossRef]
24. Skamarock, W.C.; Klemp, J.B.; Dudhia, J. *A Description of the Advanced Research WRF Version 3*; Technical Note NCAR/TN-475+STR; National Center for Atmospheric Research: Boulder, CO, USA, 2008. [CrossRef]
25. Grell, G.A.; Peckham, S.E.; Schmitz, R.; McKeen, S.A.; Frost, G.; Skamarock, W.C.; Eder, B. Fully Coupled "Online" Chemistry within the WRF Model. *Atmos. Environ.* **2005**, *39*, 6957–6975. [CrossRef]
26. Piccoli, A.; Agresti, V.; Bedogni, M.; Lonati, G.; Pirovano, G. A Bottom-up Modelling Chain to Evaluate the Impact of Urban Road Transport Policies on Air Quality and Human Health. *Urban Clim.* **2024**, *55*, 101893. [CrossRef]
27. Karamchandani, P.; Vijayaraghavan, K.; Yarwood, G. Sub-Grid Scale Plume Modeling. *Atmosphere* **2011**, *2*, 389–406. [CrossRef]
28. Karamchandani, P.; Lohman, K.; Seigneur, C. Using a Sub-Grid Scale Modeling Approach to Simulate the Transport and Fate of Toxic Air Pollutants. *Environ. Fluid Mech.* **2009**, *9*, 59–71. [CrossRef]
29. Emery, C.; Baker, K.; Wilson, G.; Yarwood, G. Comprehensive Air Quality Model with Extensions: Formulation and Evaluation for Ozone and Particulate Matter over the US. *Atmosphere* **2024**, *15*, 1158. [CrossRef]
30. Lopes, D.; Ferreira, J.; Rafael, S.; Hoi, K.I.; Li, X.; Liu, Y.; Yuen, K.-V.; Mok, K.M.; Miranda, A.I. High-Resolution Multi-Scale Air Pollution System: Evaluation of Modelling Performance and Emission Control Strategies. *J. Environ. Sci.* **2024**, *137*, 65–81. [CrossRef] [PubMed]

31. Lopes, D.; Rafael, S.; Ferreira, J.; Relvas, H.; Almeida, S.M.; Faria, T.; Martins, V.; Diapouli, E.; Manousakas, M.; Vasilatou, V.; et al. Assessing the Levels of Regulated Metals in an Urban Area: A Modelling and Experimental Approach. *Atmos. Environ.* **2022**, *290*, 119366. [CrossRef]
32. Ge, S.; Wang, S.; Xu, Q.; Ho, T. Source Apportionment Simulations of Ground-Level Ozone in Southeast Texas Employing OSAT/APCA in CAMx. *Atmos. Environ.* **2021**, *253*, 118370. [CrossRef]
33. Giani, P.; Balzarini, A.; Pirovano, G.; Gilardoni, S.; Paglione, M.; Colombi, C.; Gianelle, V.L.; Belis, C.A.; Poluzzi, V.; Lonati, G. Influence of Semi- and Intermediate-Volatile Organic Compounds (S/IVOC) Parameterizations, Volatility Distributions and Aging Schemes on Organic Aerosol Modelling in Winter Conditions. *Atmos. Environ.* **2019**, *213*, 11–24. [CrossRef]
34. Ramboll. *CAMx User's Guide Version 7.10*; Ramboll Environ International Corporation: Novato, CA, USA, 2020.
35. EPRI. *SCICHEM Version 1.2: Technical Documentation*; Final Report Prepared by ARAP/Titan Corporation, Princeton, NJ, for EPRI, Palo Alto, CA; EPRI: Palo Alto, CA, USA, 2000.
36. Seaton, M.; O'Neill, J.; Bien, B.; Hood, C.; Jackson, M.; Jackson, R.; Johnson, K.; Oades, M.; Stidworthy, A.; Stocker, J.; et al. A Multi-Model Air Quality System for Health Research: Road Model Development and Evaluation. *Environ. Model. Softw.* **2022**, *155*, 105455. [CrossRef]
37. Benavides, J.; Snyder, M.; Guevara, M.; Soret, A.; Pérez García-Pando, C.; Amato, F.; Querol, X.; Jorba, O. CALIOPE-Urban v1.0: Coupling R-LINE with a Mesoscale Air Quality Modelling System for Urban Air Quality Forecasts over Barcelona City (Spain). *Geosci. Model Dev.* **2019**, *12*, 2811–2835. [CrossRef]
38. Chen, F.; Kusaka, H.; Bornstein, R.; Ching, J.; Grimmond, C.S.B.; Grossman-Clarke, S.; Loridan, T.; Manning, K.W.; Martilli, A.; Miao, S.; et al. The Integrated WRF/Urban Modelling System: Development, Evaluation, and Applications to Urban Environmental Problems. *Int. J. Climatol.* **2011**, *31*, 273–288. [CrossRef]
39. Jia, H.; Kikumoto, H. Line Source Estimation of Environmental Pollutants Using Super-Gaussian Geometry Model and Bayesian Inference. *Environ. Res.* **2021**, *194*, 110706. [CrossRef]
40. Zhang, L.; Gong, S.; Padro, J.; Barrie, L. A Size-Segregated Particle Dry Deposition Scheme for an Atmospheric Aerosol Module. *Atmos. Environ.* **2001**, *35*, 549–560. [CrossRef]
41. Zhang, L.; Brook, J.R.; Vet, R. A Revised Parameterization for Gaseous Dry Deposition in Air-Quality Models. *Atmos. Chem. Phys.* **2003**, *3*, 2067–2082. [CrossRef]
42. ISPRA. *Italian Emission Inventory 1990–2018. Informative Inventory Report 2020*; Istituto Superiore per la Protezione e la Ricerca Ambientale: Roma, Italy, 2020.
43. ARPA Lombardia Inemar. Available online: https://www.inemar.eu/xwiki/bin/view/Inemar/HomeLombardia (accessed on 17 May 2023).
44. UNC. *SMOKE v3.5 User's Manual*; University of North Carolina at Chapel Hill: Chapel Hill, NC, USA, 2013.
45. Guenther, A.; Karl, T.; Harley, P.; Wiedinmyer, C.; Palmer, P.I.; Geron, C. Estimates of Global Terrestrial Isoprene Emissions Using MEGAN (Model of Emissions of Gases and Aerosols from Nature). *Atmos. Chem. Phys.* **2006**, *6*, 3181–3210. [CrossRef]
46. Gong, S.L. A Parameterization of Sea-Salt Aerosol Source Function for Sub- and Super-Micron Particles. *Glob. Biogeochem. Cycles* **2003**, *17*, 1097. [CrossRef]
47. Rouil, L.; Honoré, C.; Vautard, R.; Beekman, M.; Bessagnet, B.; Malherbe, L.; Meleux, F.; Dufour, A.; Elichegaray, C.; Flaud, J.M.; et al. Prev'air: An Operational Forecasting and Mapping System for Air Quality in Europe. *Bull. Am. Meteorol. Soc.* **2009**, *90*, 73–84. [CrossRef]
48. Guevara, M.; Tena, C.; Porquet, M.; Jorba, O.; Pérez García-Pando, C. HERMESv3, a Stand-Alone Multi-Scale Atmospheric Emission Modelling Framework-Part 2: The Bottom-up Module. *Geosci. Model Dev.* **2020**, *13*, 873–903. [CrossRef]
49. EMEP/EEA. *Air Pollutant Emission Inventory Guidebook 2016: Technical Guidance to Prepare National Emission Inventories*; European Environment Agency: Copenhagen, Denmark, 2016; Volume 21/2016.
50. Comune di Milano Portale Open Data | Comune Di Milano. Available online: https://dati.comune.milano.it/ (accessed on 17 May 2023).
51. Yang, C.; Gidófalvi, G. Fast Map Matching, an Algorithm Integrating Hidden Markov Model with Precomputation. *Int. J. Geogr. Inf. Sci.* **2017**, *32*, 547–570. [CrossRef]
52. Carslaw, D.C.; Ropkins, K. Openair—An R Package for Air Quality Data Analysis. *Environ. Model. Softw.* **2012**, *27–28*, 52–61. [CrossRef]
53. Janssen, S.; Thunis, P. *FAIRMODE Guidance Document on Modelling Quality Objectives and Benchmarking—Version 3.3*; Publications Office of the European Union: Luxembourg, 2022.
54. Karner, A.A.; Eisinger, D.S.; Niemeier, D.A. Near-Roadway Air Quality: Synthesizing the Findings from Real-World Data. *Environ. Sci. Technol.* **2010**, *44*, 5334–5344. [CrossRef]
55. Zhou, Y.; Levy, J.I. Factors Influencing the Spatial Extent of Mobile Source Air Pollution Impacts: A Meta-Analysis. *BMC Public Health* **2007**, *7*, 89. [CrossRef]

56. Karamchandani, P.; Koo, A.; Seigneur, C. Reduced Gas-Phase Kinetic Mechanism for Atmospheric Plume Chemistry. *Environ. Sci. Technol.* **1998**, *32*, 1709–1720. [CrossRef]
57. Berkowicz, R.; Hertel, O.; Larsen, S.E.; Sørensen, N.N.; Nielsen, M. *Modelling Traffic Pollution in Streets*; National Environmental Research Institute: Nagpur, India, 1997.
58. Valencia, A.; Venkatram, A.; Heist, D.; Carruthers, D.; Arunachalam, S. Development and Evaluation of the R-LINE Model Algorithms to Account for Chemical Transformation in the near-Road Environment. *Transp. Res. Part D Transp. Environ.* **2018**, *59*, 464–477. [CrossRef] [PubMed]
59. Venetsanos, A.G.; Vlachogiannis, D.; Papadopoulos, A.; Bartzis, J.G.; Andronopoulos, S. Studies on Pollutant Dispersion from Moving Vehicles. *Water Air Soil Pollut. Focus* **2002**, *2*, 325–337. [CrossRef]